ISSN 8755-6839

SCIENCE OF **TSUNAMI HAZARDS**

Journal of Tsunami Society International

**Volume 40 Number 2 2021**

ISSN 8755-6839

SCIENCE OF **TSUNAMI HAZARDS**

Journal of Tsunami Society International

**Volume 40 Number 2 2021**

# NUMERICAL SIMULATION OF A CATASROPHIC EARTHQUAKE AND STRONG TSUNAMI OF APRIL 1, 2014 NEAR THE NORTHWESTERN PART OF THE CHILEAN COAST

**Mazova R.Kh.[1,2], Moiseenko T.[1], Kurkin A.A.[1], Jorge Van Den Bosch F.[3], Gustavo Oses A.[3]**

*[1] Nizhny Novgorod State Technical University n.a. R.E. Alekseev, 24, Minin str., 603950 Nizhny Novgorod, Russia. e-mail address: Raissamazova@yandex.ru*
*[2]Moscow Institute of Physics and Technology (MIPT), Moscow Region, Russia*
*[3]Engineering Center Mitigation Natural Catastrophes Faculty of Engineering. Antofagasta. Chile. e-mail address: Jorge.VanDenBosch@uantof.cl; Gustavo.oses@uantof.cl*

## ABSTRACT

Catastrophic seismic events off the coast of Chile and the tsunami caused by them on April 1, 2014 north of Iquique with a magnitude of 8.2 are analyzed. Possible causes of moderate tsunami strength at a sufficiently large earthquake magnitude have been investigated. Within the framework of the keyboard block model of the subduction zone, based on the data on the localization of the main shock and aftershocks, the structure of the seismic source was selected. It was found that the computation results for the tsunami run-up noticeably exceed the observational data, which may be associated with the complex dynamics of the source. Comparison with the data of computations of other authors is performed.

***Keywords:*** *tsunami, seismic and tsunami dangers, tsunamigenic earthquakes, tsunami waves, numerical simulation, Chilean coast.*

## 1. INTRODUCTION

One of the strongest recent earthquakes, followed by a strong tsunami, occurred on April 1, 2014 with a magnitude of $M$ = 8.2 off the coast of northern Chile, 95 km northwest of Iquique. The tsunami hit the coast of Chile, causing significant damage. The epicenter of the mega-earthquake was in the subduction zone along the Peru-Chilean Trench, where the Nazca plate subducts under the South American plate at a convergence rate of about 65-80 mm / year. The nature of the generated tsunami waves in this zone, their propagation and behavior in the coastal zone have been analyzed in sufficient detail in the literature (see, e.g., (Brodsky and Lay, 2014; Catalan et al, 2015; Fritz et al., 2011; Hamlington et al., 2011; Hayes et al., 2012; Omira et al., 2016; Ramirez et al., 1997; Ruiz et al., 2016; Shrivastava et al., 2016; Zaytsev et al., 2016). Chile is in one of the most seismically active regions of the world - every day in northern Chile there are 15-30 weak shocks. Such a high level of seismic activity is associated with the geological structure of the northern part of Chile, where there is a deep-sea trench near the coast (up to 3000 m deep). However, there is also a very flat continental a slope that extends 150 km from the coast to the trench, forming a terrace.

The need to consider a more complex earthquake source for the Chilean subduction zone, adequate to the realization of aftershocks during an earthquake, was shown in our previous works (Mazova and Ramirez, 1999; Lobkovsky et.al., 2006). Historical records indicate that a series of catastrophic tsunamigenic earthquakes (Catalan et al., 2015; Omira et al., 2016) regularly occur off the coast of Chile. One of them occurred on August 13, 1868 with a maximum magnitude $M$ = 8.5 in the southern region of Peru, when the earthquake source extended to the northern coast of Chile, near the city of Arica, which caused a strong tsunami, which later is referred to as the "tsunami in Arica". The epicenter of the earthquake was located less than 100 km of the coast, on the terrace of a deep-sea trench and in almost all coastal points where the tsunami was recorded, it began with the withdrawal of water from the coast, followed by a train of waves, in which the second wave was the most destructive. Tsunami waves caused by this earthquake reached a maximum coastal height of up to 21 m. The tsunami that occurred during the Chilean earthquake of 1868 reached the shores of New Zealand. Also, on May 10, 1877, a devastating earthquake with a magnitude of $M$ = 8.8 occurred with a source off the northern coast of Chile, which was accompanied by a catastrophic tsunami. In the literature, this tsunami is referred to as the "Iquique tsunami". In the city of Iquique, the height of waves on the coast reached 4.8 m, and at various points on the coast of South America, tsunami waves hit the coast with a height of up to 24 m. Whole city blocks were washed away and destroyed.

In the 20th century, three catastrophic earthquakes accompanied by tsunamis also occurred on the coast of Chile, of which two occurred in central and northern Chile. Thus, on August 16, 1906, an earthquake with a magnitude of $M$ = 7.8 occurred in the central and northern parts of the Chilean coast. The greatest damage was done to the city of Valparaiso. The maximum heights of tsunami waves along the coast reached 3.5 m. The runup to the coast proceeded moderately, in the form of coastal flooding. On May 22, 1960, a destructive mega-earthquake occurred with a source in the southern part of central Chile with a magnitude of $M$ = 9.5. The maximum rise of water on the Chilean coast reached 25 m.

At the beginning of the 21st century, the strongest earthquakes occurred in the middle and northern parts of the Chilean coast. For example, on February 27, 2010, a catastrophic earthquake of magnitude $M = 8.8$ occurred off the coast of Chile, which caused a powerful tsunami (Pararas-Carayannis, 2010; Fritz et al., 2011; Hamlington et al., 2011; Hayes et al., 2012; Omira et al., 2016; Zaytsev et al., 2016). The source of the earthquake (35.909 ° S, 72.733 ° W) was in the sea at a depth of 35 km under the earth's crust, 17 km from the coastal settlements of Curanipe and Cobquecura, 90 km of the capital of Bio-Bio Concepcion, 150 km northwest of Concepcion and 63 km southwest of Cauquenes. An earthquake in Chile caused a powerful tsunami - twenty minutes after the earthquake, a sea wave two meters high struck the coast of Chile.

The strong earthquake on April 1, 2014 in northern Chile, off the Chilean coast, struck an area of a historic seismic gap called the gap in northern Chile (or the "Iquique gap"), which has experienced 5 major earthquakes every 114 years on average over the past 574 years, all with records of devastating tsunamis for cities in northern Chile and southern Peru, and some devastating impact on the Pacific Ocean. For the tsunamis that occurred in northern Chile in 1868 and 1877 (see above), there are tide gauge records of that time at Fort Point California USA, (see Fig. 1), where it can be seen other tsunamis that occurred in the north, central and southern parts of Chile where the largest tsunami from 1960 to 1922 stands out, the smallest registered by this old station.

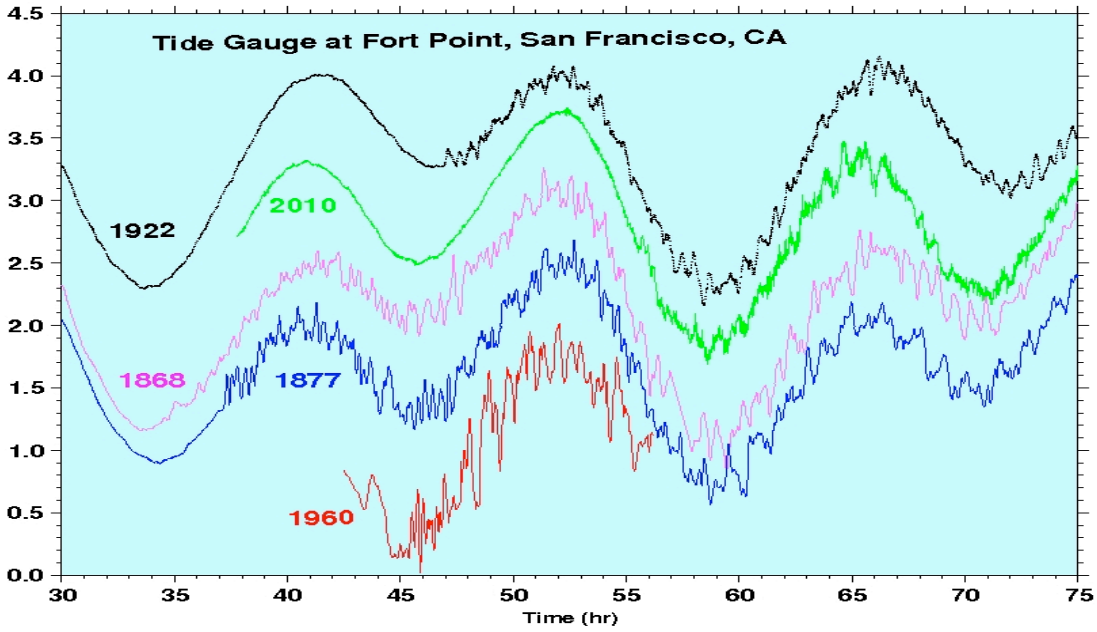


*Fig. 1. Barrientos S. Wards S. 2008. (Private communication)*

## 2. EARTHQUAKE AND TSUNAMI OF 01.04.2014 NEAR THE NORTHWESTERN PART OF THE CHILEAN COAST

It is important to note that the considered earthquake was preceded by an increasing seismicity and was directed from south to north (Internet resource ECDM_20140402_Chile_Earthquake). In this regard, during March 2014, shortly before the earthquake on April 1, 14 earthquakes-precursors occurred in the rupture zone; 3 earthquakes from 4.5º to 4.9º, 7 earthquakes from 5.1º to 5.8º and finally, very close to April 1, there were 4 earthquakes from 6.2º to 6.7º. This is likely a historical pattern of earthquakes preceding a major earthquake in this area.

This paper analyzes the catastrophic seismic event off the northern part of the Chilean coast on April 1, 2014. In the area of the city of Iquique, the epicenter of an earthquake with a magnitude of $M = 8.2$ was located in the region of 20.518° S and 70.498° W, a seismic fault called the northern Chilean or "Iquique seismic fault." Tsunami waves were recorded on the Chilean coast in cities: Pisagua - 1.7 m; Yunin - 1.7 m; Iquique - 1.6 m; Punta Negra - 1.6 m; Alto Hospice - 1.6 m; Chucumata - 1.3 m; Arica - 0.7 m. These data, as well as publicly available data on aftershocks, formed the basis of this study. Data on seismic activity in the Chilean subduction zone in 2014, leading to the occurrence of strong tsunamis that repeatedly hit the Chilean coast and leading to destruction are presented in Table 1.

**Table 1. Earthquakes and tsunamis on the coast of Chile for 2014 event.**

| Date and time | Geographic coordinates | Magni-tudes | Region, contributed magnitudes and comments | Nearby cities |
|---|---|---|---|---|
| 2014-04-03 02:43:14 UTC | 20.518°S 70.498°W | 7,7 | Northern Chile. This earthquake is an aftershock of the $M = 8.2$ subduction zone earthquake that occurred April 1, 2014. The $M = 8.2$ event triggered a tsunami with measured heights near 2 meters along the northern Chile and southern Peru coasts. Since the $M = 8.2$ event, 47 aftershocks ranging from $M = 4.2$ to this M 7.8 event have occurred, including a M 6.4 on April 2. | 1. 49km (30mi) SW of Iquique, Chile<br>2. 177km (110mi) N of Tocopilla, Chile<br>3. 227km (141mi) S of Arica, Chile<br>4. 269km (167mi) NW of Calama, Chile<br>5. 509km (316mi) SSW of La Paz, Bolivia |
| 2014-04-01 23:57:57 UTC | 19.898°S 70.924°W | 6,9 | Northern Chile. | 1. 89km (55mi) WNW of Iquique, Chile<br>2. 170km (106mi) SSW of Arica, Chile<br>3. 221km (137mi) SSW of Tacna, Peru<br>4. 253km (157mi) S of Ilo, Peru<br>5. 476km (296mi) SW of La Paz, Bolivia |
| 2014-04-01 23:46:46 UTC | 19.642°S 70.817°W | 8,2 | Northern Chile.<br>The April 1, 2014 $M = 8.2$ earthquake in northern Chile occurred as the result of thrust faulting at shallow depths near the Chilean coast.<br>The April 1 earthquake occurred in a | 1. 95km (59mi) NW of Iquique, Chile<br>2. 139km (86mi) SSW of Arica, Chile<br>3. 190km (118mi) SSW of Tacna, Peru |

| | | | | |
|---|---|---|---|---|
| | | | region of historic seismic quiescence – termed the northern Chile or Iquique seismic gap. Historical records indicate a $M$ = 8.8 earthquake occurred within the Iquique gap in 1877, which was preceded immediately to the north by an $M$ = 8.8 earthquake in 1868. | 4. 228km (142mi) SSE of Ilo, Peru<br>5. 447km (278mi) SW of La Paz, Bolivia |
| 2014-03-16 21:16:30 UTC | 19.925°S 70.628°W | 6,7 | Northern Chile. This earthquake is considered the last precursor of the 8.2º major earthquake on April 1, 2014 in this area (Internet resource ECDM_20140402_Chile_ Earthquake). | 1. 60km (37mi) WNW of Iquique, Chile<br>2. 164km (102mi) SSW of Arica, Chile<br>3. 216km (134mi) S of Tacna, Peru<br>4. 244km (152mi) N of Tocopilla, Chile<br>5. 460km (286mi) SW of La Paz, Bolivia |

## 3. SEISMIC SOURCE MODEL FOR THE APRIL 1, 2014 CHILEAN EARTHQUAKE

Figure 2 shows the localization of the source of the April 1, 2014 earthquake in northern Chile and aftershocks in the next 2 days after the main shock, as well as the data of the tide gauge in Patach. The epicenter of the earthquakes was in the region of 20.518 ° S and 70.498 ° W. Tsunami waves have been recorded on the Chilean coast in a number of cities (see above).

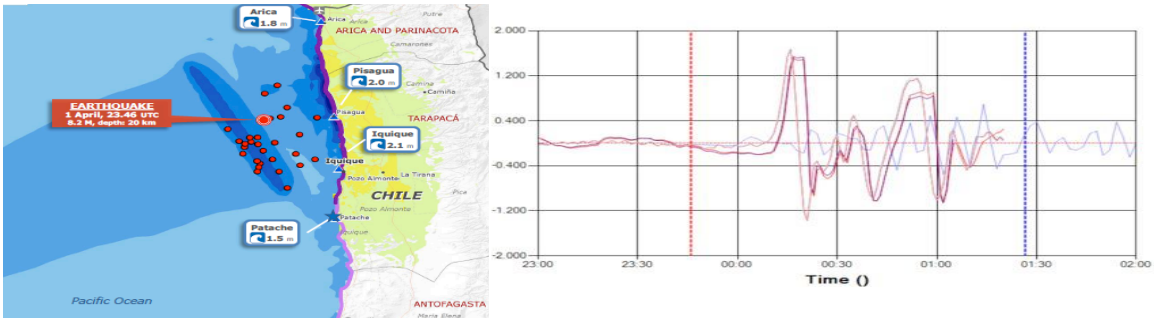


a) b)

*Fig. 2. a) Localization of the earthquake source and the location of aftershocks in the next 2 days after the main shock; b) data from a tide gauge in Patache (Internet resource ECDM_20140402_ Chile_Earthquake [20]).*

In this paper, to carry out numerical modeling of this earthquake, a three-block seismic source with a size of 110 × 230 km is considered. (Fig. 3). The area of the source is 25300 km$^2$; the height of the maximum vertical rise is 4 m (see Table 2). If we take into account the localization and time of aftershocks, then the shape of the source will have a more complex form (see Fig.3). In accordance with the seismic process in the source, the movement of the keyboard blocks is defined in Table 2.

**Table 2. Characteristics of simulated sources (Scenario 1).**

| Block number | 1 | 2 | 3 |
|---|---|---|---|
| Heights (m) | 2 | 4 | 1 |
| Movement start time (s) | 90 | 0 | 40 |
| Movement final time (s) | 120 | 40 | 90 |

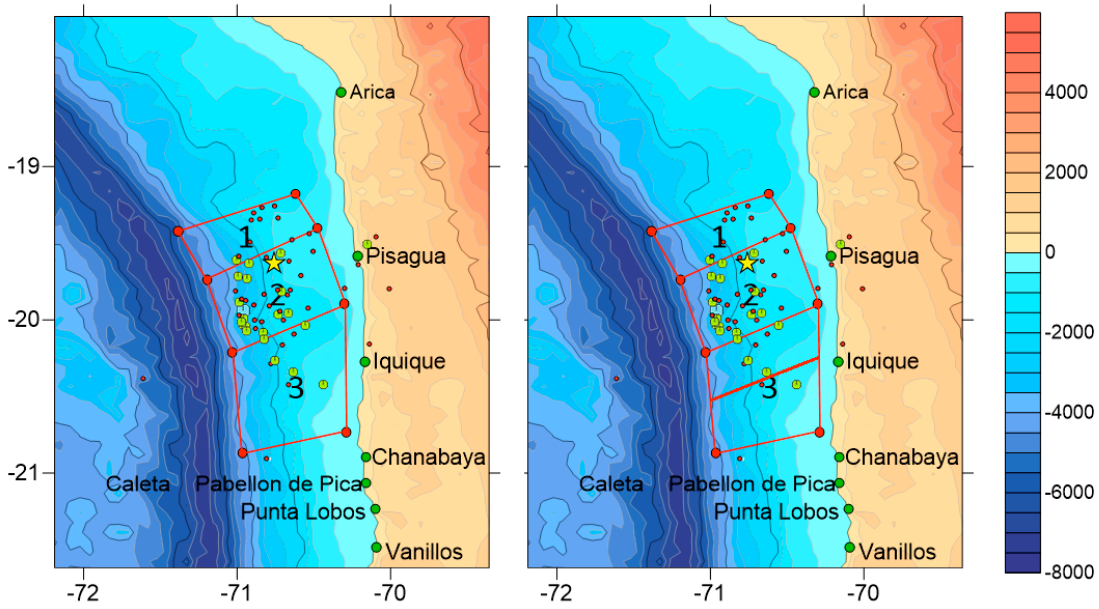


*a)* *b)*

*Fig. 3. The shape of the earthquake source of April 1, 2014: a) for 3-block seismic source (Scenario 1); for 4-block seismic source (Scenario 2).*

## 4. MATHEMATICAL STATEMENT OF THE PROBLEM

To simulate the generation and propagation of tsunami waves from an earthquake, a scenario was adopted that was selected according to the direction of seismic activity. For numerical simulation of a tsunami from a seismic source located along the Chilean coast, a part of the Pacific Ocean basin in the square of 600-900 E. and 50-400 S was used. To describe the process of wave generation and propagation in accordance with the assumptions made above, a system of nonlinear shallow water equations is used (see, for example, (Mazova et al., 2006; Voltsinger et al., 1989).

$$\begin{cases} \vec{U}_t + \vec{U} \cdot grad\ \vec{U} + g \cdot grad\,\eta = 0 \\ \eta_t + div\left((H + \eta - B)\vec{U}\right) = B_t \end{cases} \qquad \vec{U} = \begin{pmatrix} u \\ v \end{pmatrix}$$

Here the functions $u$ and $v$ are the velocities of the water particles; $g$ is the acceleration of gravity, $B(x, y, t)$ is a function that describes the law of motion of the basin bottom when

simulating the dynamics of the displacement of the Earth's crust in the earthquake source (within the framework of the key-block model of the earthquake source). Under this simulation a modernized finite-difference scheme (Sielecki and Wurtele, 1970) (see, for example, (Lobkovsky et al., 2019)) was used.

## 5. RESULTS OF NUMERICAL SIMULATION

Figure 4 shows the characteristic moments during the generation of the tsunami source by the selected seismic source for three points in time corresponding to the movement of three key blocks.

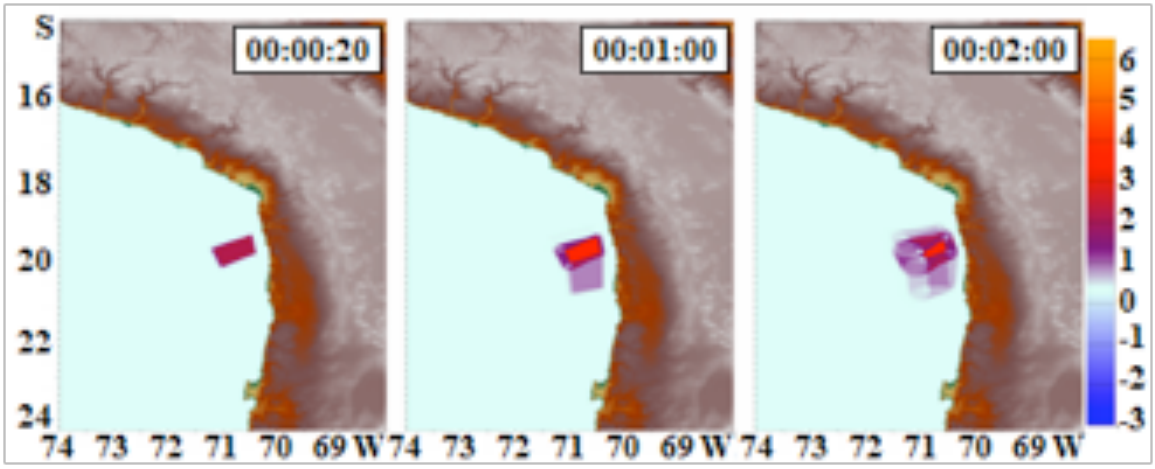


*Fig. 4. The generation of a tsunami source*

Figure 5 shows the process of wave propagation over the water area for 9 points in time. For this formulation of the problem, the process of wave propagation is considered on a part of the Pacific Ocean: along the central part of the Chilean coast. For this scenario, Fig. 6 shows the distribution of the maximum wave heights over the computed water area. It can be seen that the highest wave heights are localized in the area of the earthquake source, while along the coast, wave heights of 5-6 m are possible. Analysis of the results shows that the highest wave heights were recorded in the central part of the water area.

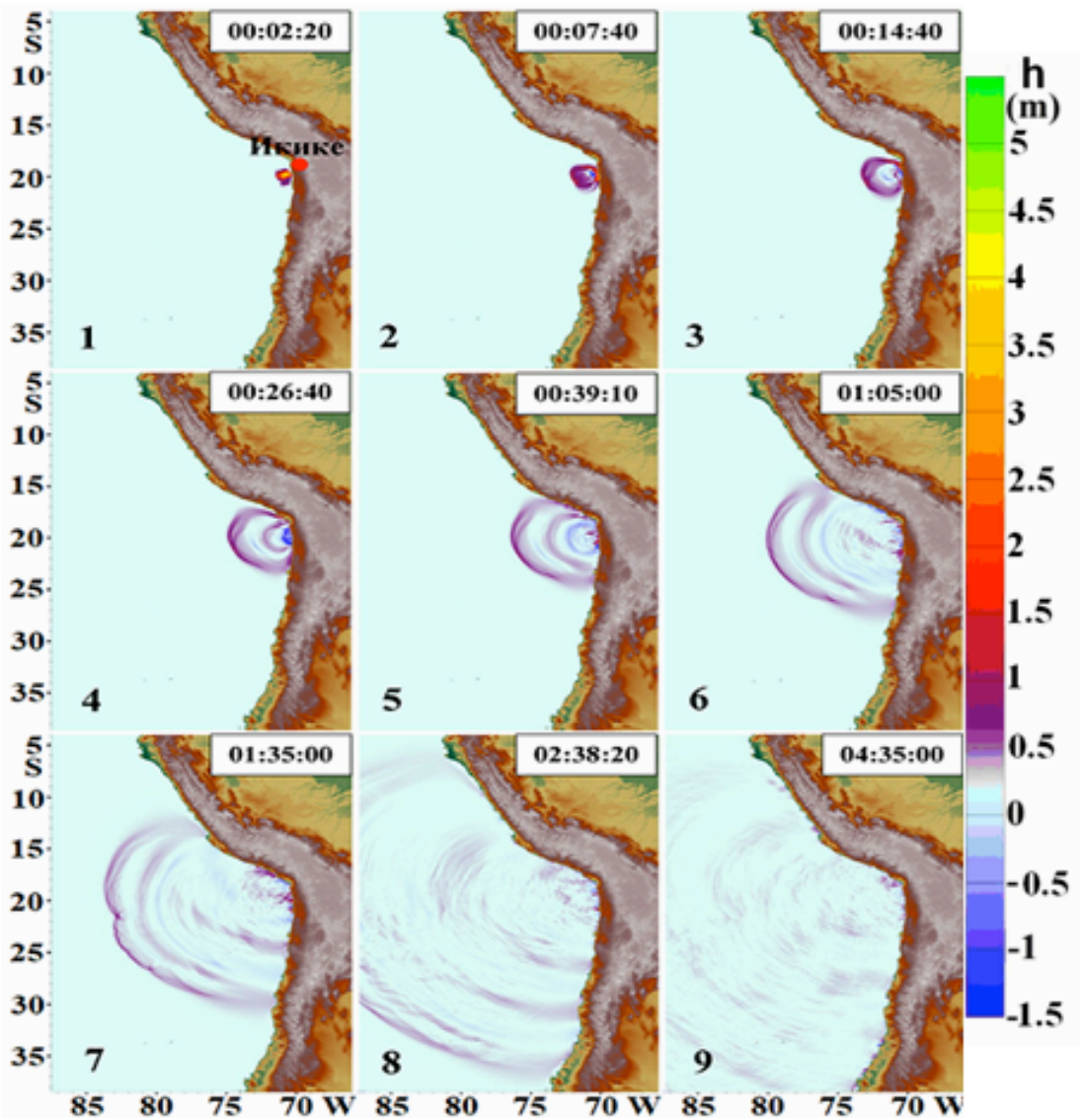


*Fig. 5. Propagation of a tsunami waves by a 3-block seismic source for the 9 time moments (Scenario 1).*

Figures 7 and 8 show a histogram for central Chile and southern Peru. It is clearly seen that the maximum heights for the central part of Chile reach 6m, and for the southern coast of Peru up to 5m.

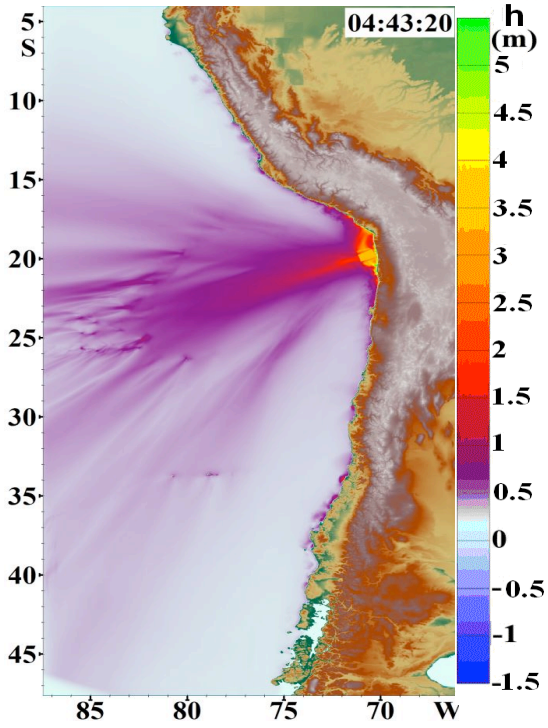


*Fig. 6. Distribution of maximum wave heights for a part of this water area according to the results of numerical simulation under Scenario 1.*

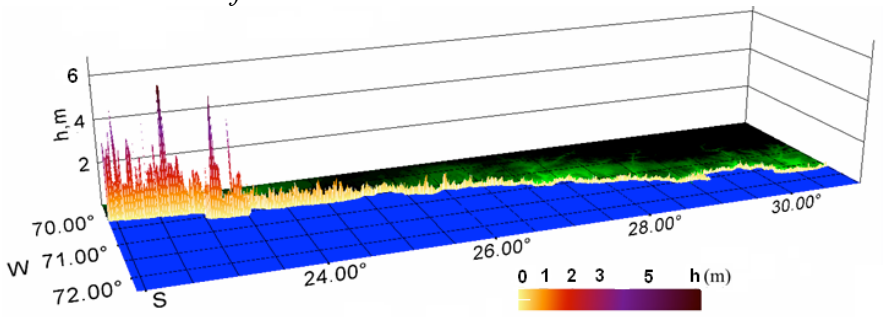


*Fig. 7. 3D histogram for central part of Chile (Scenario 1).*

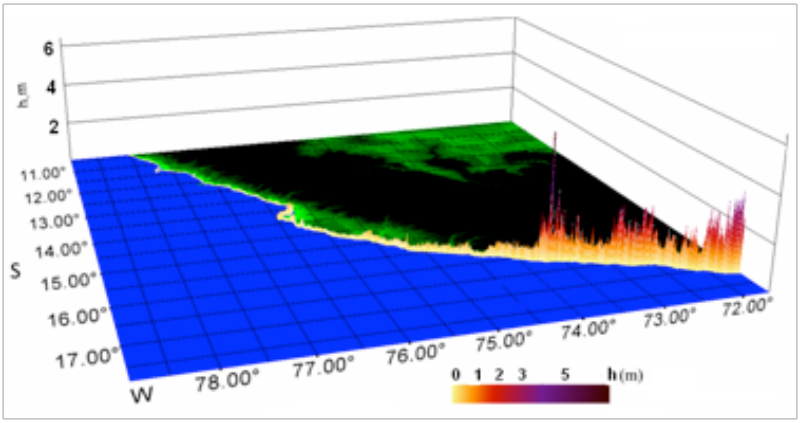


*Fig. 8. 3D histogram for southern coast of Peru (Scenario 1).*

Table 3 shows the computed data on the height of tsunami waves at the 10-meter isobath along the Chilean coast in the area of the computational domain. It can be seen that with the selected geometry and structure of the source, as well as for the given dynamics of the key blocks, the greatest runup value is obtained for pp. Iquique, Pisagua, Arica, and Tocopilla, and with distance from the source, the runup value decreases, reaching 1.6 m for Taltal and 0.8 m for Paposo on both sides of the source.

**Table 3. Results of numerical simulation of runup heights (Scenario 1)**

| Point | Field-data heights , m | Numerical simulation, m |
|---|---|---|
| Matarani (72.11°W 17.02°S) | 0.6 | 1.6 |
| Arica (70.29°W 18.47°S) | 1.65 | 3.7 |
| Caleta Camarones (70.26°W 19.18°S) | - | - |
| Pisagua (70.2°W 19.6°S) | 2.3 | 4.3 |
| Iquique (70.1°W 20.2°S) | 1.8 | 5.2 |
| Patache (70.2°W 20.8°S) | 1.7 | - |
| Tocopilla (70.19°W 22.08°S) | 1.5 | 3.2 |
| Mejillones (70.45°W 23.1°S) | 0.7 | 1.6 |
| Antofagasta (70.39°W 23.65°S) | 0.35 | 1.1 |
| Paposo (70.46°W 25.01°S) | 0.35 | 0,8 |
| Taltal (70.48°W 25.4°S) | 0.35 | 1,1 |
| Chanaral (71.58°W 29.03°S) | 0.5 | - |

To correct the results obtained, a numerical simulation was performed for a four-block earthquake source (see Fig. 3b).

**Table 4. Characteristics of simulated sources (Scenario 2).**

| Block number | **1** | **2** | **3** | **4** |
|---|---|---|---|---|
| Heights (m) | **1.2** | **1.6** | **1.3** | **1.5** |
| Movement start time (s) | **30** | **0** | **60** | **100** |
| Movement final time (s) | **60** | **30** | **100** | **120** |

Figure 9 shows three characteristic time moments under generation of the tsunami source by the selected seismic source.

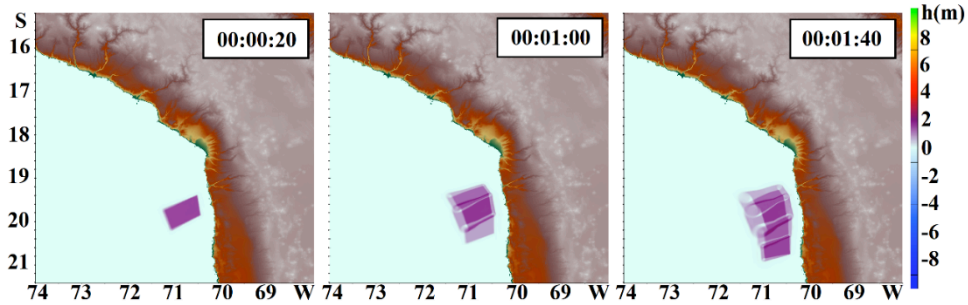


*Fig. 9. The generation of a tsunami source.*

For this scenario, Fig. 10 shows the distribution of the maximum wave heights over the computed water area.

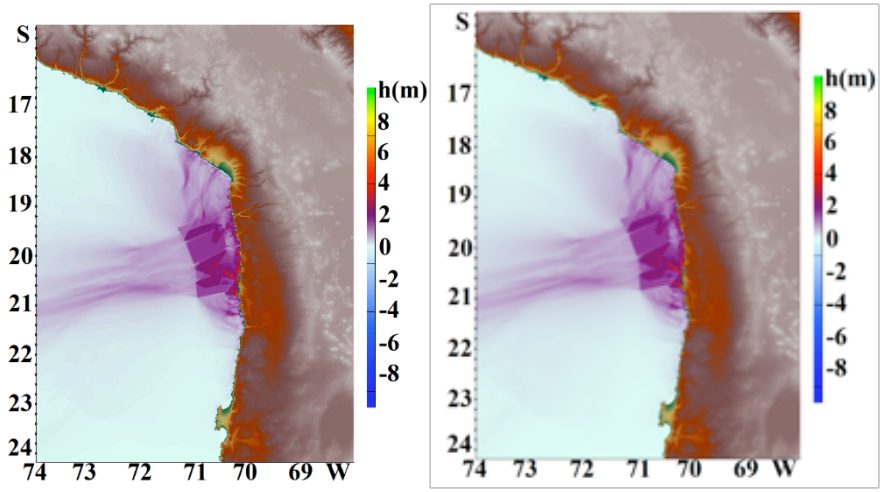


*Fig. 10. Distribution of maximum wave heights for a part of this water area according to the results of numerical simulation under Scenario 2.*

Figure 11 shows a 2D histogram for central Chile. It is clearly seen that the maximum heights for the central part of Chile are somewhat higher than 5m.

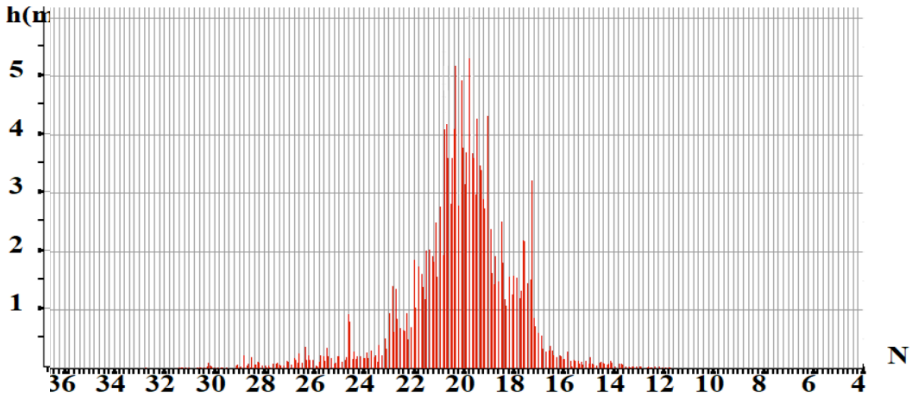


*Fig. 11. 2D histogram for central Chile (Scenario 2).*

The computation results for Scenario 2 and comparison with field data and computations for Scenario 1 are shown in Table 5. It can be seen that with the chosen geometry and structure of the source, as well as for the dynamics of the key blocks for Scenario 2, there is a good agreement with the field data. The deviation from the field data is available only for the Pisagua and Iquique points, which is obviously related to the shape of the source.

**Table 5. Comparison of field-data and computed heights**

| № | Points | Field-data heights , m | Numerical simulation, m ( Scenario 1) | Numerical simulation, m ( Scenario 2) |
|---|---|---|---|---|
| 1 | **Matarani** (72.11°W 17.02°S) | 0.6 | 1.6 | 0.6 |
| 2 | **Arica** (70.29°W 18.47°S) | 1.65 | 3.7 | 1.8 |
| 3 | **Caleta Camarones** (70.26°W 19.18°S) | - | - | 3.48 |
| 4 | **Pisagua** (70.2°W 19.6°S) | 2.3 | 4.3 | 3,5 |
| 5 | **Iquique** (70.1°W 20.2°S) | 1.8 | 5.2 | 2,8 |
| 6 | **Patache** (70.2°W 20.8°S) | 1.7 | - | 1.95 |
| 7 | **Tocopilla** (70.19°W 22.08°S) | 1.5 | 3.2 | 0.7 |
| 8 | **Mejillones** (70.45°W 23.1°S) | 0.7 | 1.6 | 0.35 |
| 9 | **Antofagasta** (70.39°W 23.65°S) | 0.35 | 1.1 | 0.3 |
| 10 | **Paposo** (70.46°W 25.01°S) | 0.35 | - | 0.2 |
| 11 | **Taltal** (70.48°W 25.4°S) | 0.35 | - | 0.2 |
| 12 | **Chanaral** (70.64 °W 26.35 °S) | 0.5 | - | 0.37 |

## 6. DISCUSSION

The results comparing the obtained computations (Scenario 1) with empirical data and computations by other authors are shown in Fig.9 and Table 4. Figure 9 shows a comparison of the computed results with field data and data from (Catalan et.al, 2015). It can be seen that the histogram of the distribution of the maximum wave heights is close to the empirical data in terms of the nature of the distribution, the wave heights are closest in the interval along the coast between 23_S and 18_S, but the computation data for the chosen scenario (Table 3) at some points is significantly higher than the field data (Table 4, column 1).

The data given in Table 3, field data, and data from (Catalan et.al, 2015) on the Chile earthquake and tsunami, 2014 are summarized in Table 4. It can be seen that the data on numerical simulation given in Scenario 1 are consistent with real data, taking values close to empirical data only in a limited number of points. This can be explained by the fact that the dynamics of blocks in the source was determined primarily by the nature of bottom bathymetry with aftershocks of the first day of the earthquake. As can be seen from the Table, the computed heights in the cited work (Catalan et.al, 2015) are significantly higher than the observational ones. It should be noted here that the observed runup heights themselves in this case are rather moderate for such strong earthquakes.

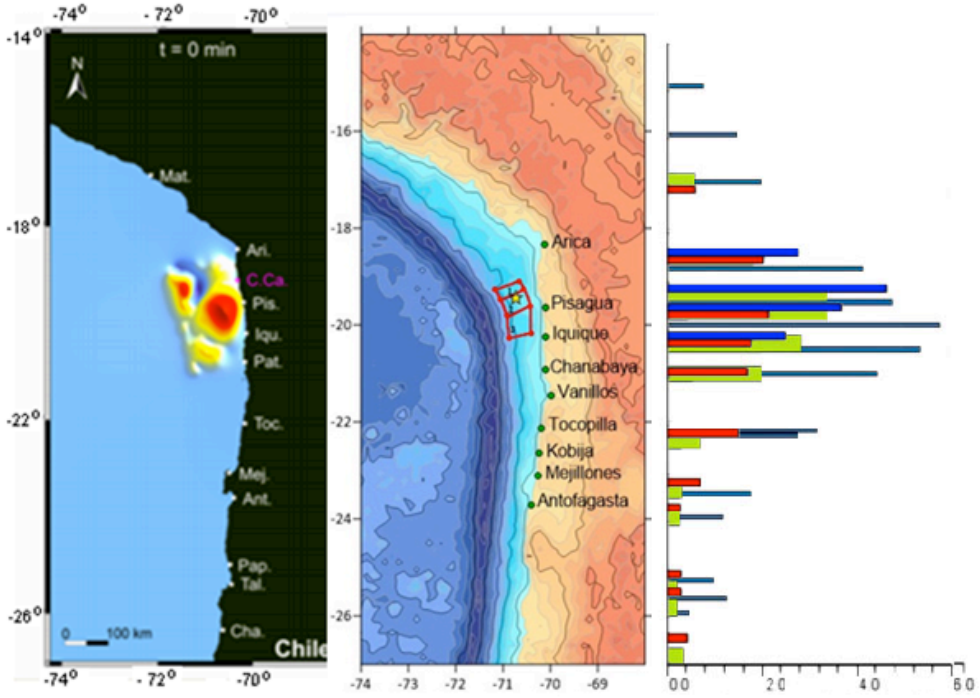


*Fig. 9. Comparison of computed and natural data for two model of seismic source for Chilean 2014 earthquake and tsunami event. Red lines – natural data; blue lines – data from work (Catalan et.al.,2015); grey lines – computation on Scenario 1; green lines – computation on Scenario 2.*

A comparative analysis with the data of works (Catalan et al., 2015; Omira et al., 2016; Ruiz et al., 2016; Shrivastava et al., 2016; Zaytsev et al., 2016) shows that the facts given in these works are somewhat contradictory, and there is little reliable information, which did not allow us to set a more adequate dynamics of blocks in the earthquake source. In (Ruiz et al., 2016) it is noted that, depending on the model of the seismic source for a given earthquake, numerical modeling gives the values of the maximum wave heights in the range from 5 to 40 m, and the average values lie in the region of 10 m, which is significantly higher than the observed values.

**Table 4. Comparison of field-data and computed heights**

| Point | Field-data heights , m | Computed heights, m [Catalan et.al., 2015] | Numerical simulation, m (Scenario 2) |
|---|---|---|---|
| Matarani (72.11°W 17.02°S) | 0.6 | - | 0.6 |
| Arica (70.29°W 18.47°S) | 1.65 | 2.9 | 1.8 |
| Caleta Camarones (70.26°W 19.18°S) | - | 4.7 | 3.48 |
| Pisagua (70.2°W 19.6°S) | 2.3 | 3.7 | 3,5 |
| Iquique (70.1°W 20.2°S) | 1.8 | 2.6 | 2,8 |
| Patache (70.2°W 20.8°S) | 1.7 | - | 1.95 |
| Tocopilla (70.19°W 22.08°S) | 1.5 | - | 0.7 |
| Mejillones (70.45°W 23.1°S) | 0.7 | - | 0.35 |
| Antofagasta (70.39°W 23.65°S) | 0.35 | - | 0.3 |
| Paposo (70.46°W 25.01°S) | 0.35 | 1 | 0.2 |
| Taltal (70.48°W 25.4°S) | 0.35 | 0,5 | 0.2 |
| Chanaral (71.58°W 29.03°S) | 0.5 | - | 0.37 |

## 7. CONCLUSIONS

As previously predicted by a number of authors (see, for example, (Mazova and Soloviev, 1994)), seismic activity along the perimeter of the Pacific Ocean will significantly increase by the end of the 20th - beginning of the 21st centuries. Indeed, there was a series of catastrophic earthquakes accompanied by a tsunami: in the Indian Ocean near Sumatra on December 26, 2004 with a magnitude of 9.1, an earthquake and tsunami on November 15, 2006 in the Kuril-Kamchatka region, a catastrophic earthquake with a magnitude of 8.8, which occurred in middle part of Chile on February 27, 2010, a tsunamigenic catastrophic earthquake in Japan on March 11, 2011 with a magnitude of 9.2 and the last event - a strong earthquake and tsunami in northern Chile in April 1 January 2014 with a magnitude of 8.2. The nature of the generated tsunami waves for each of these events, their propagation and behavior in the coastal zone have been analyzed in sufficient detail in the literature (see above).

As follows from the works on the analysis of the ratio of the earthquake magnitude and tsunami run-up height, a complex earthquake source without taking into account the geodynamics in the seismic source and taking into account the effects of the coastal zone, gives higher heights than a monoblock (see, for example, Kurkin et al., 2004; Lukhnov et al., 2006; Tyatyushkina et al., 2020; Yalciner et al., 2007; Zaitsev et al., 2020). This conclusion also follows from a number of recent works (Ruiz et al., 2015, Catalan et al., 2016, Omira et al., 2016; Zaytsev et al., 2016). For example, in (Ruiz et al., 2015), the potential possibility of a new earthquake in a large seismic gap along northern Chile was considered, where the Pisagua earthquake occurred on April 1, 2014, which destroyed the middle segment of this gap, leaving the southern and northern segments not destroyed. So this region has a large area that can generate an earthquake with $M > 8.5$ and a strong tsunami. In their numerical modeling, they took a magnitude $M = 9$ in northern Chile and calculated the vertical co-seismic static displacement, adding up the elementary "sections". The paper analyzes a number of chaotic fault models, taking into account the nonplanar geometry of the fault in northern Chile. Numerical results in some cases show the maximum run-up of 30-40 m. Instead, the minimum run-up coincides with homogeneous (monoblock) models of the order of 4 m. In the latter case, there is an underestimation by a factor of 6. Analysis shows that models with a lot of slip near the trough are likely to produce higher runups than other scenarios. In (Catalan et al., 2016), a numerical simulation of the tsunami on April 1, 2014, caused by an earthquake with a magnitude $M =$ 8.2 near the coast of northern Chile, was carried out. The analysis of the characteristics of this tsunami was carried out on the basis of a comparison of the results of numerical simulation with field data. Despite the large magnitude of the earthquake, the tsunami was moderate, with a relatively uniform distribution of runup - the runup peak was 4.6 m. This is explained by the authors with the concentration of the maximum slip achieved at an intermediate depth on the fault, resulting in a rapid decay of the tsunami energy. The temporal evolution of a tsunami is changing - there are places where tsunami energy is conserved, while in other places tsunami energy increases over time after an earthquake. The authors believe that this is the result of the interaction of long-period standing oscillations and the activity of a trapped edge wave controlled by the inner slopes of the shelf.

In (Omira et al., 2016; Zaytsev et al., 2016), the relationship between the generation and propagation of tsunamis in the near-field zone and coseismic deformation was investigated for three recent (2010, 2014 and 2015) earthquake and tsunami events in the deep-water region of Peru-Chilean Trench. These three earthquakes were found to be due to faults with important extensions under the continent, which result in tsunamis with short wavelengths, relative to the width of the faults involved, and with reduced initial potential energy. In addition, the presence of the Chilean continental margin, which includes a shallow bathymetry shelf and a continental slope, inhibits tsunami propagation and coastal impact. All these factors contribute to the concentration of the local impact, but may, on the other hand, reduce the effects of the tsunami in the far-field zone from earthquakes along the Peru-Chile Trench.

Thus, the study carried out in this work confirms the need to consider the source of an earthquake of a more complex shape, taking into account the geodynamic processes in the source, adequate implementation of the aftershock process during an earthquake and taking into account the effects of the coastal zone, as was shown in our previous works (Lobkovsky et al., 2006; Mazova et al., 2014, Lobkovsky et al., 2017, Lobkovsky et al., 2019, Lobkovsky et al., 2021).

## ACKNOWLEDGEMENTS

The authors acknowledge the funding of this study provided by grant of President of the Russian Federation for the state support of Leading Scientific Schools of the Russian Federation (Grant No. NSH-2485.2020.5).

## REFERENCES

Brodsky E.E. and Thome Lay, (2014) *Recognizing Foreshocks from the 1 April 2014 Chile Earthquake* // Science. 344, 700.

Catalan P.A. et al. (2015) *The April 01, 2014, Pisagua Tsunami: Observations and Modeling* // American Geophysical Union.

Dunbar P., Stroker K., Heather McCullough (2010). *Do the 2010 Haiti and Chile earthquakes and tsunamis indicate increasing trends?* // Geomatics, Natural Hazards and Risk 1 95-114.

Fritz H.M. et al. (2011) *Field Survey of the 27 February 2010 Chile Tsunami* // Pure Appl. Geophys. 168 , 1989–2010

Hamlington, B.D., R.R. Leben, O.A. Godin, J.F. Legeais, E. Gica, and V.V. Titov: (2011) *Detection of the 2010 Chilean tsunami using satellite altimetry*. Nat. Hazards Earth Syst. Sci., 11, doi: 10.5194/nhess-11-2391-2011, 2391–2406.

Hayes G.P. et al. (2012) *Slab1.0: A three-dimensional model of global subduction zone geometries* // J. Geophys. Res.,. 117, B01302, Internet resource ECDM_20140402_ Chile_Earthquake.

Kurkin A.A., Zaitsev A.I., Yalchiner A., Pelinovsky E.N. (2004) *Modified computer complex "Tsunami" for assessing the risks associated with tsunami* // Izvestia of the Academy of Engineering Sciences named after A.M. Prokhorov. V. 9. P. 88-100.

Lobkovsky L.I. Geodynamics of spreading, subduction and two-level plate tectonics zones // Nauka Press, Moscow, USSR, 1988.

Lobkovsky L.I., Baranov BV. Keyboard model of strong earthquakes in island arcs and active continental margins // Doklady of the Academy of Sciences of the USSR. V. 275. № 4. P. 843-847. 1984.

Lobkovsky L.I., Nikishin A.M., Khain V.E. Current problems of geotectonics and geodynamics // Nauchnyi Mir Press, Moscow, Russia, 2004.

Lobkovsky, L. I., Mazova, R. Kh, Kataeva, L Yu., & Baranov, B.V. (2006) Generation and propagation of catastrophic tsunami in the basin of Sea of Okhotsk. Possible scenarios, // Doklady, V.410, 528–531.

Lobkovsky L., I.Garagash, B.Baranov, R.Mazova, N.Baranova. (2017) *Modeling Features of Both the Rupture Process and the Local Tsunami Wave Field from the 2011 Tohoku Earthquake* // Pure Appl. Geophys. V.174, P.3919-3938, doi:10.1007/s00024-017-1539-5 p.1-20.

Lobkovsky L.I., I. A. Garagash, R. Kh. Mazova. (2019) *Numerical simulation of tsunami waves generated by the underwater landslide for the Northern Coast of the Black Sea (Dzhubga Area*) // Geophys. J. Int. V.218, P.1298–1306, https://doi.org/10.1093/ gji/ ggz221).

Lukhnov A.O., Chernov A.G., Kurkin A.A., Polukhina O.E. (2006) *Problems of creating a hardware-software complex for studying the hydrodynamics of the shelf zone..*// Izvestiya of the Academy of Engineering Sciences. A.M. Prokhorov. V.18, P. 120-123.

Mazova R.Kh. Soloviev S.L.. (1994) *On influence of sign of leading tsunami wave on runup height on the coast* // Sci.Tsunami Hazards V.12, P. 25-31.

Mazova R.Kh, Ramirez J.F. (1999) *Tsunami waves with an initial negative wave on the Chilean coast //* Natural Hazards V.20, P83-92.

Mazova R.Kh., B.V. Baranov, L.I. Lobkovsky, N.A. Baranova, K.A.Dozorova, O.N. Chaykina. (2014) *Numerical Model Study of Possible Earthquake – Generated Tsunami in Komandorsky Seismic Gap, Western Aleutian Island Arc* // Sci.Tsunami Haz. V.32, 131–155.

Mendosa Carlos, (USGS) "Basic Seismology for Geotechnics, Construction and Risks", course. Faculty of Engineering. University of Antofagasta. 6-7 Nov 1997. (private communication).

Murty T.C. Seismic Sea Waves: Tsunami // Dept. of Fisher. and the Environ., FMS: Ottawa Canada, 1977

Omira R. et al. (2016) *Tsunami Characteristics Along the Peru–Chile Trench: Analysis of the 2015 Mw8.3 Illapel, the 2014 Mw8.2 Iquique and the 2010 Mw8.8 Maule Tsunamis in the Near-field* // Pure Appl. Geophys. V.173, 1063–1077

Pararas-Carayannis G. *The earthquake and tsunami of 27 February 2010 in Chile - Evaluation of source mechanism and of near- and far-field tsunami effects* // Sci.Tsunami Hazards 29 (2010) 96-126.

Pelinovsky, E.N., Soloviev, S.L., Mazova, R.Kh. *Statistical data on the character of the run-up of tsunami waves* // Oceanology 23 (1983) 932-937.

Pelinovsky E.N. & Mazova R.Kh., 1992, *Exact analytical solution of nonlinear problems of tsunami wave runup on slopes with different profiles* // Natural Hazards, 6, 227-249

Pritchard M.E., M. Simons, P. A. Rosen, S. Hensley and F. H. Webb. (2002) *Co-seismic slip from the 1995 July 30 Mw =8.1 Antofagasta, Chile, earthquake as constrained by InSAR and GPS observations* // Geophys. J. Int. V.150, 362–376.

Ramirez, J. Titichoca, H. Lander J. and Whiteside L. (1997) *The minor destructive tsunami occurring near Antofagsta, northen Chile, july 30 1995*, Science of Tsunami Hazards, V.15, No. 1. Hawaii USA.

Ruiz J.A. et al. (2015) *Numerical simulation of tsunami runup in northern Chile based on non-uniform k22 slip distributions* // Nat Hazards 79:1177–1198.

Shrivastava M.N. et al. *Earthquake segmentation in northern Chile correlates with curved plate geometry* // Sci.Rep.

Sielecki, A., and M. Wurtele, (1970) The numerical integration of the nonlinear shallow water equations with sloping boundaries // J.Comput. Phys., V.6, P.219, doi:10.1016/0021- 9991(70)90022-7.

Tyatyushkina E., Kozelkov A., Kurulin V., Plygunova K., Utkin D., Kurkin A., Pelinovsky E. (2020) *Verification of the Logos software package for tsunami simulations* // Geosciences (Switzerland). V. 10. № 10. P. 1-28.

Urzúa U. Luis "Arica Puerta Nueva" 3° Edición. Editorial Andrés Bello. Santiago Chile. 1969

Yalciner A.C., Ozer C., Karakus H., Ozyurt G., Pelinovsky E., Zaitsev A., Kurkin A. (2007) *Modeling and visualization of tsunamis: Mediterranean examples* // In: Tsunami and Nonlinear Waves. P. 273-283.

Voltsinger N.E., Klevanny K.A. & Pelinovsky E.N., 1989, *Long-Wave Dynamics of Coastal Zone*, Gidrometeoizdat, Leningrad, USSR, (in Russian).

Zaytsev O. et al. (2016) *A Comparative Analysis of Coastal and Open-Ocean Records of the Great Chilean Tsunamis of 2010, 2014 and 2015 off the Coast of Mexico* // Pure Appl. Geophys. V.173, 4139–4178.

Zaytsev A.I., Kurkin A.A., Pelinovsky E.N., Yalçıner A. (2020) *The Use of the NAMI-DANCE Computational Complex on the Problem of Tsunami Waves* // J.Appl. Mech. and Tech. Phys. V.61. No. 7. P. 1140–1152.

ISSN 8755-6839

SCIENCE OF TSUNAMI HAZARDS

Journal of Tsunami Society International

Volume 40 Number 2 2021

# TSUNAMIS FROM STRIKE-SLIP AND NORMAL EARTHQUAKES AND ITS RELATION WITH THE PRODUCT OF DOMINANT PERIOD AND DURATION OF MORE THAN 50 SECONDS OF EARTHQUAKE *P*-WAVE

**Madlazim[1], Tjipto Prastowo[1], Muhammad Nurul Fahmi[1], Dyah Permata Sari[1], Ella Melianda[2], Sorja Koesuma[3]**

[1]*Universitas Negeri Surabaya, Surabaya 60231, Indonesia*
[2]*Universitas Syiah Kuala, Aceh, Indonesia*
[3]*Universitas Sebelas Maret, Surakarta, Indonesia*
*E-mail: madlazim@unesa.ac.id*

## ABSTRACT

It is widely known that earthquakes with strike-slip or normal-faulting crustal displacements have generated destructive tsunamis around the world. Many researchers have proposed that the main cause of such events was due to factors not associated with tsunami-seismic parameters. However, the present study examines a correlation between tsunamis generated by strike-slip or normal-faulting earthquake events and their associated two tsunami-seismic parameters, namely the dominant period $T$d and the duration of more than 50 seconds, $T$50ex of earthquake P-wave, and compares these with tsunami event validity (TEV). Based on this analysis, we confirm a correlation between tsunamis generated by strike-slip or normal-faulting earthquake events with periods $T\text{d} \times T\text{50ex} \geq 10$ s. Thus, we propose that major earthquakes with both strike-slip and normal-fault motions, have the potential to generate more effectively tsunamis when the rupture duration is ≥ 50 seconds and *P*-wave dominant periods have values of $T\text{d} \times T\text{50ex} \geq 10$s.

***Keywords***: *Tsunami-seismic parameters; P-*wave *Dominant period; P-*wave *duration of more than 50 seconds; Tsunami event validity; strike-slip, normal-faulting earthquakes.*

## 1. INTRODUCTION

Tsunamis are usually generated by the release of seismic energy on the earth's upper crust, which results in displacements of the sea floor, referred to as earthquake sources. However, besides tectonic mechanisms, tsunamis can be also generated from volcanic sources and submarine landslides (Ward, 2011). Large tsunamis are rarely generated by earthquakes associated with strike-slip or normal-faulting motions. This is due to the fact that strike-slip faults involve primarily horizontal and not vertical crustal movements of the sea floor. Small local tsunamis that may be generated only correlate to insignificantly localized seafloor deformation in size (Gusman *et al*., 2017; Lay *et al*., 2017).

However, historical records indicate that small tsunamis have been generated by strike-slip earthquakes as, for example, that of the 1906 San Francisco, California event (Ma *et al*., 1991; Thatcher *et al*., 1997) and the 1994 Mindoro, Philippines (Imamura *et al*., 1995). Similarly, small tsunamis were generated by more recent events such as the 2016 Kaikoura, New Zealand (Power *et al*., 2017; Ulrich *et al*., 2019a), and the 28 September 2018 Palu, Indonesia earthquakes (Carvajal *et al*., 2019; Ulrich *et al*., 2019b; Madlazim et al., 2020). However, for that Palu earthquake, the major cause of the destructive tsunami remained debatable, since both strike-slip and normal-faulting mechanisms were equally considered responsible. For this event, it has been further proposed that a collateral co-seismic event, such as an undersea landslide may have been a likely source contributing to generation of the tsunami.

Recent work (Muhari *et al*., 2018; Carvajal *et al*., 2019; Heidarzadeh *et al*., 2019) advocated also that a submarine landslide which followed the *M*w 7.5 earthquake on land, disturbed the sea surface and was responsible for the extreme tsunami run-up heights at several places in Palu Bay. Contrary to this, Ulrich *et al*. (2019b) proposed a model of co-seismic earthquake parameters to find an oblique component in addition to a slip faulting type for the event, causing a significant vertical seafloor displacement of 1.5 m across a segment underneath Palu-Koro fault. This finding was supported by aerial evidence from satellite imagery, confirming surface deformation associated with the event and its corresponding ruptured segment (Madlazim and Supriyono, 2014; Socquet *et al*., 2019). Furthermore, other studies (Goda *et al*., 2019; Gusman *et al*., 2019) argued for a combined source mechanism of vertical seafloor displacement and a complex undersea landslide following mainshocks. Using the combined source model, they successfully resolved the surveyed run-up heights and the corresponding tsunami inundation, as documented by the subsequent field surveys.

Using both duration more than 50 seconds, $\tau_{50ex}$ and the dominant period, $\tau_d$ acquired from teleseismic data, Lomax and Michelini (2009b; 2011) showed that the parameters could be potential tsunami discriminants. Madlazim *et al*. (2013), using local Indonesian events, confirmed the importance of the parameters on assessing tsunami hazard. Regarding the dependence of tsunami excitation on seafloor displacement, Lomax and Michelini (2013) further used these parameters for effective early warning within five minutes. Using a total of 300 Indonesian events, independently of source mechanisms, Madlazim *et al*. (2019) made this limitation shortened by a minute with no false warning in the reported case studies .

Although a better understanding of reliable tsunami discriminants for rapid analysis and assessment of tsunami potential has developed in time, the roles played by tsunami importance $\Lambda$ first defined in Lomax and Michelini (2009b) and the product of $\tau_d \times \tau_{50ex}$ discussed in Lomax and Michelini (2011), along with the inclusion of earthquake characterization, remain questionable for accurate tsunami early warning. In particular, a correlation between tsunamigenic earthquakes of strike-slip or normal-faulting origin and the corresponding tsunamis induced in terms of probability to occur, in percentage, for a set of seismic data given for both source mechanisms, independent of epicenter location, is of paramount importance. Knowledge about this issue may help parameterize tsunami excitation aftershocks, hence improve the reliability of tsunami early warning. Therefore, this study aims to analyze past tsunamis around the world generated by strike-slip and normal earthquakes' and its relation with the product of dominant period and duration more than 50 seconds of earthquake *P*-wave.

## 2. METHODS

Estimates of $\tau_d$ were performed using a direct procedure with no inversion at the initiation, making the calculation process relatively shortened. The first step of $\tau_d$ estimates were to determine time domain $\tau_c$ according to Lomax and Michelini (2011) as follows,

$$\tau_c = 2\pi T2 T1 v2 dt dT2 T1 \acute{v}2 dt \quad (1)$$

where $T1$ = 0 (the onset time of *P*-waves) and $T2$ = 55 s acquired from teleseismic data (Lomax and Michelini, 2009). Detailed steps of $\tau_d$ estimates are as follows: (1) preparing raw earthquake data records from the vertical velocity component of broadband seismogram in a miniseed format, (2) applying 4-poles and a corner frequency of 0.05 Hz Butterworth bandpass filter to obtain the high-frequency, vertical component of velocity records for each seismic station; (3) picking *P*-wave arrival times automatically at the high-frequency, vertical-velocity seismogram; (4) integrating the seismogram and comparing it with vertical acceleration component of broadband seismogram times $2\pi$ of arrival times of *P*-waves automatically picked up from the vertical-velocity records on the high-frequency seismogram; and (5) the final results were values of $\tau_d$.

$$T_{50Ex} = A_{50}/A_{RMS} \quad (2)$$

Where $A_{50}$ is average amplitude for 50 to 60 seconds, and $A_{RMS}$ is average amplitude for 0 to 25 seconds.

The followings are detailed steps of determining the $\bar{\tau}50ex$ exceeding 50 s using a direct procedure: (1) preparing raw data from the vertical component of broadband seismogram in a miniseed format, (2) applying 4-poles and the 5-20 Hz Butterworth band pass filter to obtain the high-frequency, vertical component of seismic velocity for each seismic station used; (3) picking arrival times of *P*-waves automatically at the high-frequency, vertical-velocity seismogram; (4) calculating the RMS-amplitude and $\bar{\tau}50$ values; and (5) estimating $\bar{\tau}50ex$ using the ratio of $\bar{\tau}50$ to the RMS-amplitude values.

The estimated values for $\tau_d$, and $\bar{\tau}50ex$ are compared with Tsunami Event Validity (TEV). Validity of the actual tsunami occurrence is indicated by a numerical rating of the reports of that event: -1 is erroneous entry indication of erroneous entry, 0 is indication of event that only caused a seiche or disturbance in an inland river, 1 is indication of very doubtful tsunami, 2 is indication of questionable tsunami, 3 is indication of probable tsunami, and 4 is indication of definite tsunami (National Geophysical Data Center / World Data Service: NCEI/WDS Global Historical Tsunami Database. NOAA National Centers for Environmental Information. doi:10.7289/V5PN93H7). The detailed algorithms above for calculations of $\tau_d$, and $\bar{\tau}50ex$ were implemented into Jokotingkir, a programming package that Madlazim *et al*. (2019) used both local and regional events to accurately calculate the three seismic parameters for improved tsunami early warning within four minutes after the main shocks, which can be accessed at http://prediksi-tsunami.unesa.ac.id/www/

The product of $\tau_d \times \bar{\tau}50ex$ was chosen here as it was proved to bring more information about potentially induced tsunamis by earthquakes than other discriminants, the moment magnitude $M_w$ (both are included in Table 1 but are then excluded in calculations for cross-correlation techniques presented in the current work). As pointed out by Necmioglu and Özel (2014), rupture duration determination has a relatively large uncertainty affecting tsunami initiation and hence being improper for tsunami hazard assessment. A similar situation to occur was found for earthquake magnitude, scaled with any measure,

as the magnitude was proved to be inaccurate for tsunami analysis and assessment (Madlazim and Prastowo, 2016). The data were acquired from a network of seismic stations on the basis of local observations available from the Indonesian Agency for Geophysics, Climatology, and Meteorology (BMKG) at http://202.90.198.100/webdc3/, regional and teleseismic data provided by the German Research Centre for Geosciences, known as GEOFON GFZ accessed at http://eida.gfz-potsdam.de/webdc3/ and the Incorporated Research Institutions for Seismology-Data Management Center (IRIS-DMC) available at http://www.iris.edu/wilber3/find_event. We used direct procedures of calculation for relatively quick assessment of tsunami generation potential using earthquake source parameters, including the dominant period $\tau_d$, the rupture duration $\tau_{dur}$ and the apparent rupture duration $\tau_{50ex}$ longer than 50 s from velocity records on the high-frequency *P*-waves seismogram.Top of Form Bottom of Form

## 3. RESULTS AND DISCUSSIONS

We considered how estimates of $\tau_d$ and $\tau_{50ex}$ were carried out. These events are associated with the movement of a left-lateral strike-slip and normal fault system in the world. Estimation of $\tau_d$ and $T_{50Ex}$ was performed using the direct procedure previously presented. Note that all the observed values for $\tau_{dvand}$ $\tau_{50ex}$ estimates are higher than their respective thresholds at $\tau_d \geq 10$ s and $\tau_{50ex} \geq 1$, respectively, for tsunami generation potential proposed by Lomax and Michelini (2011). The same finding as field observations, and both eyewitnesses and video-footages collected (Carvajal *et al*., 2019; Goda *et al*., 2019).

Our tasks now are examining earthquake datasets from all the events considered in this study and classifying them using the two sensitive correlation parameters for tsunami excitation, namely $\tau_d \times \tau_{50ex} \geq 10$ s. We are here intent to use global tsunamigenic earthquake datasets to test whether such requirement holds for strike-slip or normal-faulting mechanisms around the globe. Each event was monitored by nearby stations locate at, on average, 478.87 km and far stations situated in, on average, 1922.66 km away from the epicenter. Each event was recorded at >25 stations at epicentral distances of $10^o - 60^o$. The point to make is that the discriminant $\tau_d \times \tau_{50ex}$ is used to examine the independence of the events on a further catastrophe, *i.e*., the events being not always followed by landslides. A total of 35 events consisting of 19 strike-slip and 16 normal-faulting mechanisms, centered either on the mainland or at sea, were analyzed, and the results were then provided in detail in Table 1. For each event, $\tau_d \times \tau_{50ex}$ was first determined after rapid calculations of $\tau_d$ and $\tau_{50ex}$. The next step was to correlate the product of $\tau_d \times \tau_{50ex}$ to TEV $\geq 3$ of the same event whether they both fulfill $\tau_d \times \tau_{50ex} \geq 10$ s. When one of these does not meet the requirement, we can then say they are not correlated.

**Table 1.** Tsunami parameter estimation results from strike-slip and normal-faulting earthquakes

| No | Origin Time (UTC) | Lat | Long | $D$ (km) | $M$ w | $T$d (s) | $T$50 ex | $T$d × $T$50ex (s) | TEV | Event | Type | Status |
|---|---|---|---|---|---|---|---|---|---|---|---|---|
| 1 | 19941114 19:15:30 | 13.5° N | 121.1° E | 31.5 | 7.0 | 5.7 | 0.8 | 4.7 | 4 | nT | So | FW |
| 2 | 19990817 00:01:38 | 40.7° N | 29.9° E | 17.0 | 7.6 | 16.8 | 1.8 | 30.4 | 4 | T | Sc | TW |
| 3 | 20021010 10:50:22 | 1.7° S | 134.3° E | 24.8 | 7.5 | 8.0 | 1.6 | 9.3 | 1 | nT | So | TW |
| 4 | 20090528 08:24:48 | 16.8° N | 86.2° W | 29.0 | 7.3 | 10.2 | 1.4 | 14.2 | 4 | T | So | TW |
| 5 | 20100112 21:53:10 | 18.4° N | 72.6° W | 15 | 7 | 3.7 | 1.5 | 5.6 | 4 | T | Sc | TW |
| 6 | 20100226 20:31 | 25.9° N | 128.4° E | 25.0 | 7.0 | 6.6 | 0.4 | 2.9 | 3 | nT | So | FW |
| 7 | 20101225 13:16:38 | 19.8° S | 167.9° E | 15.7 | 7.3 | 11.5 | 1.5 | 16.9 | 4 | T | No | TW |
| 8 | 20110109 10:03:43 | 19.3° S | 168.4° E | 20.7 | 6.5 | 5.6 | 1.7 | 10.5 | 4 | T | No | TW |
| 9 | 20110510 08:55:12 | 20.3° S | 168.3° E | 33.4 | 6.8 | 9.2 | 1.0 | 11.5 | 4 | T | No | TW |
| 10. | 20110624 03:09:38 | 51.9° N | 171.8° W | 49.8 | 7.3 | 5.1 | 1.9 | 12.8 | 4 | T | No | TW |
| 11 | 20110706 19:03:2 | 29.3° S | 176.2° W | 25.4 | 7.6 | 10.2 | 2.1 | 21.2 | 4 | T | No | TW |
| 12 | 20110710 00:57:10 | 38.1° N | 143.3° E | 24.7 | 7.0 | 5.4 | 1.5 | 11.0 | 4 | T | No | TW |
| 13 | 20120202 13:34:41 | 17.8° S | 167.2° E | 27.3 | 7.0 | 7.1 | 1.3 | 10.1 | 4 | T | No | TW |
| 14 | 20120309 07:09:53 | 19.2° S | 169.8° E | 33.7 | 6.6 | 6.7 | 0.9 | 12.5 | 4 | T | No | TW |
| 15 | 20120411 08:38:37 | 2.2° N | 93.0° E | 26.3 | 8.6 | 9.4 | 1.9 | 18.3 | 4 | T | So | TW |
| 16 | 20120411 10:43:10 | 0.8° N | 92.4° E | 21.6 | 8.2 | 7.8 | 2.0 | 15.8 | 4 | T | So | TW |
| 17 | 20130105 08:58:19 | 55.2 ° N | 134.8 ° W | 3.1 | 7.5 | 14.1 | 1.6 | 22.5 | 4 | T | So | TW |
| 18. | 20130208 15:26:38 | 10.9° S | 166.2° E | 22.4 | 7.0 | 4.9 | 1.6 | 8.1 | 4 | nT | So | FW |
| 19. | 20130419 03:05:52 | 46.1° N | 150.9° E | 109 | 7.2 | 2.8 | 2.8 | 7.8 | 2 | nT | No | TW |

| No | Origin Time (UTC) | Lat | Long | $D$ (km) | $M$ w | $T$d (s) | $T50$ ex | $T$d × $T50$ex (s) | TEV | Event | Type | Status |
|---|---|---|---|---|---|---|---|---|---|---|---|---|
| 20 | 20141014 03:51:37 | 12.5° N | 88.1° W | 63.9 | 7.3 | 4.8 | 1.4 | 13.7 | 4 | T | No | TW |
| 21 | 20150710 04:12:42 | 9.3° S | 158.3° E | 20.0 | 6.7 | 7.2 | 1.1 | 7.8 | 4 | T | So | TW |
| 22 | 20150718 02:27:32 | 10.4° S | 165.1° E | 11.8 | 6.9 | 9.3 | 1.7 | 15.9 | 4 | T | No | TW |
| 23 | 20160302 12:49:48 | 4.95° S | 94.3° E | 24.0 | 7.8 | 8.4 | 2.0 | 17.1 | 4 | T | So | TW |
| 24 | 20160812 01:26:36 | 22.4° S | 173.1° E | 16.44 | 7.2 | 9.4 | 1.1 | 10.7 | 4 | T | So | TW |
| 25 | 20161121 20:59:49 | 37.3° N | 141.4° E | 11.35 | 6.9 | 8.8 | 2.3 | 19.9 | 4 | T | No | TW |
| 26 | 20161113 11:02:59 | 42.7° S | 173.1° E | 22.0 | 7.8 | 11.0 | 1.9 | 20.8 | 4 | T | Sc | TW |
| 27 | 20170103 21:52:30 | 19.3° S | 176.1° E | 126.9 | 6.9 | 9.5 | 0.7 | 13.9 | 4 | T | No | TW |
| 28 | 20170717 23:34:13 | 54.4° N | 168.8° E | 10.99 | 7.7 | 7.6 | 1.6 | 12.3 | 4 | T | So | TW |
| 29 | 20170908 04:49:20 | 15.0° N | 93.9° W | 56.67 | 8.1 | 7.2 | 2.4 | 17.2 | 4 | T | No | TW |
| 30 | 20180110 02:51:31 | 17.4° N | 83.5° W | 10 | 7.5 | 11.1 | 1.8 | 20.2 | 4 | T | So | TW |
| 31 | 20180123 09:31:42 | 56.0° N | 149.0° W | 25 | 7.9 | 2.7 | 2.6 | 6.9 | 4 | nT | So | FW |
| 32 | 20180928 10:02:43 | 0.2° S | 119.8° E | 10.0 | 7.5 | 8.4 | 1.9 | 15.9 | 4 | T | Sc | TW |
| 33 | 20181211 02:26:32 | 58.5° S | 26.5° W | 164.6 | 7.1 | 10.4 | 1.7 | 18.1 | 0 | T | No | FW |
| 34 | 20181205 04:18:08 | 21.9° S | 169.4° E | 10 | 7.5 | 8.6 | 1.5 | 12.9 | 4 | T | No | TW |
| 35 | 20200128 19:10:24 | 19.4° N | 78.8° W | 14.8 | 7.7 | 8.8 | 1.7 | 14.7 | 4 | T | So | TW |

Notes: Sc (Continental Strike-Slip Fault), So (Oceanic Strike-Slip Fault), Nc (Continental Normal Fault), No (Oceanic Normal Fault), FW (False Warning = unrelated), TW (True Warning = related), T (Tsunami), nT (non Tsunami).

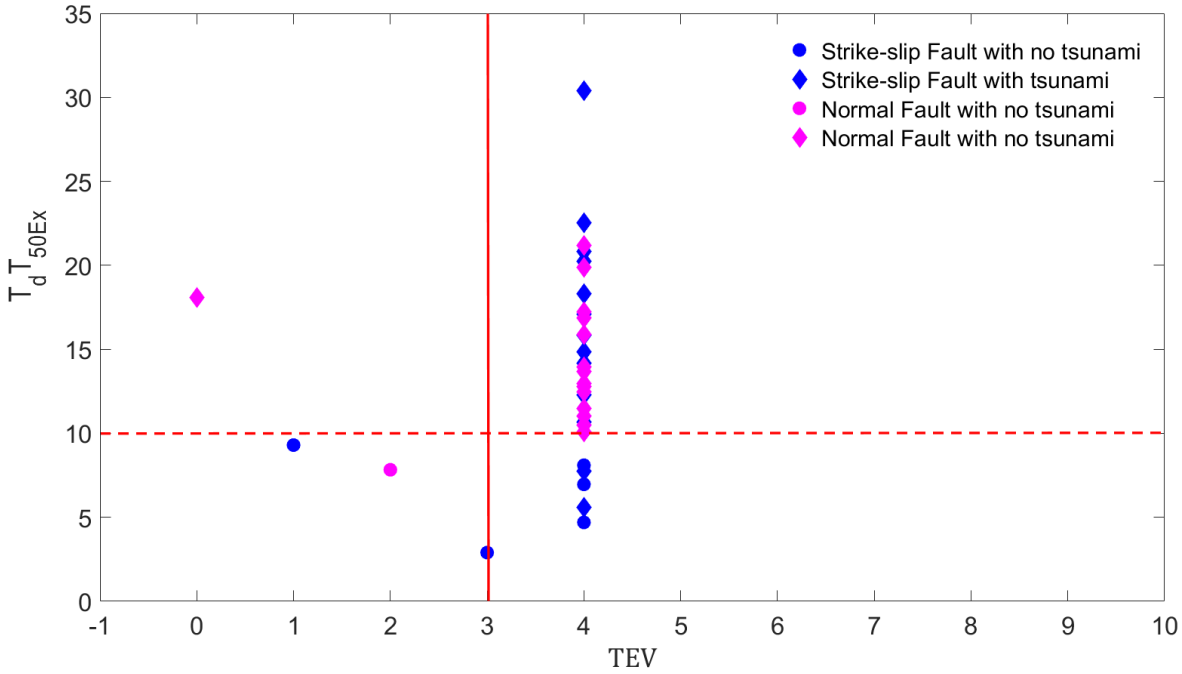


Fig 1. The relationship between $T_d \times T_{50ex}$ and TEV. The vertical red line shows the threshold value of TEV and the horizontal red line shows threshold value of $T_d \times T_{50ex}$. diamond shows a tsunami event and a circle shows a non-tsunami event.

In Fig. 1 for strike-slip cases, there exist 15 events where $T_d \times T_{50ex} \geq 10$ s and TEV $\geq 3$ are satisfied and related, leaving the requirement unrelated for other 4 events in this type of energy release mechanism. While, for normal-faulting, almost all, which are 15 of 16, show a positive correlation. From a total of 35 events considered, about 86% of all the events, or 30 occurrences, take both the requirement simultaneously. These include 15 strike-slip and 14 normal-faulting mechanisms. It follows that both mechanisms can be potential sources of tsunami generation as long as the requirement meets and in particular, rupture movement is directed towards the seafloor. This finding also provides insight into a possibility that the tsunamigenic earthquake, independent of source mechanism, is then possibly centered on land or at sea. A well-known example of this is a tsunami wave that hit Kaikoura region in New Zealand on 13 November 2016 (Power *et al*., 2017; Ulrich *et al*., 2019a) several minutes after the main shock occurred in the region. Another example from a recent local event is the one when a propagating tsunami wave penetrating into Palu Bay on the 28 September 2018 Palu, Indonesia (Carvajal *et al*., 2019; Ulrich *et al*., 2019b).

Cases where $T_d \times T_{50ex}$ and TEV $< 3$ are uncorrelated, meaning that only one of these relations $T_d \times T_{50ex} \geq 10$ s or TEV $\geq 3$ is satisfied, are accounted for a total of 9 earthquake events consisting of 8 events due to strike-slips and one event related to normal-faulting. For a special case where $T_d \times T_{50ex} \geq 10$ s does not hold but TEV $\geq 3$ is satisfied; we here argue for some possible factors that are not related to seismic source parameters, for example, an underwater landslide, inducing tsunami generation. In oppose to this, for a situation where $T_d \times T_{50ex} \geq 10$ s holds but TEV $\geq 3$ is no longer the case; the possible reason is that a tsunami wave is generated at a location in the open ocean far away from beaches and propagates towards the shorelines with much reduction in its wave energy. Hence, when the wave approaches near the shorelines, its height is measured by local tide-gauges insignificantly, causing no much destruction on areas near the shores.

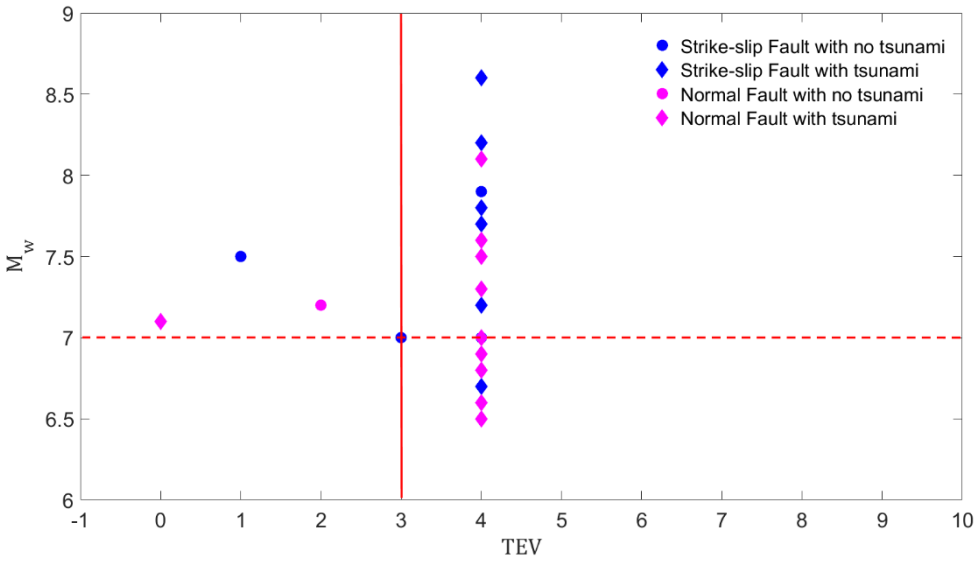


Fig 2. The relationship between *M*w and TEV. The vertical red line shows the threshold value of TEV and the horizontal red line shows threshold value of *Mw*. Triangle shows a tsunami event and a circle shows a non-tsunami event.

If viewed from the correlation between the parameters Mw and TEV as in Figure 2, for the case of the strike-slip earthquake from 19 events there are 10 events that fulfill these two parameters and the other 9 only fulfill one of them. Meanwhile, in normal earthquake cases, there are also 10 correlated events and 6 not. If in the total of the entire event, there are 71% or as many as 24 earthquakes that meet the requirements for the Mw and TEV parameters. If the two parameters are correlated, it can be said that the tsunami that occurred was caused by a large magnitude earthquake which had an amplitude of more than 0.5 m and could have occurred near the coastline, while for cases where only the Mw parameter was met it means that the tsunami wave was likely generated at a location in the open ocean far from the coast and spreading to the shoreline with much reduction in wave energy so that the amplitude is less than 0.5 m, and for cases where only the TEV is satisfied there may be other sources affecting TEV $\geq 3$, one example is an underwater landslide.

**Table 2.** The calculation results of tsunami potential use different discriminants

| Discriminant | Available (min after OT) | Treshold Value | True Warning | | | False warning | | |
|---|---|---|---|---|---|---|---|---|
| | | | TEV$\geq$3 | TEV < 3 | %** | TEV$\geq$3 | TEV < 3 | %** |
| $M_w$ | 5-10 | 7.0 | 24 | 1 | 71% | 7 | 3 | 29% |
| $\tau d \times \bar{\tau} 50ex$ | 5 | 10.0 | 28 | 2 | 86% | 4 | 1 | 14% |

** Percent of true warning and false warning

Table 2 shows that the correlation of parameters $\tau d \times \bar{\tau} 50ex$ and TEV correctly identifies 86% of the tsunami events caused by strike-slip earthquakes and normal earthquakes, more than the correlation of $M_w$ and TEV which is only 71%. This is because the Mw parameter cannot identify earthquakes that have a magitude moment of less than 7.0 which have a long rupture duration (Lomax and Michelini, 2009A). Therefore, the parameter $\tau d \times \bar{\tau} 50ex$ is better used than the parameter Mw for tsunami early warning.

## 4. CONCLUSIONS

We have examined two tsunami-seismic parameters, the dominant period $T_d$ and the likely apparent rupture-duration $T_{50ex}$ that exceeds 50 s in the form of a calculated value $T_d \times T_{50ex}$ and a value characterizing tsunami importance $I_t$. We have then used these values as good measures considering $T_d \times T_{50ex} \geq 10$ s generation using a total of 35 earthquakes initiated by 19 strike-slip and 16 normal-faulting movements of varying source locations worldwide. Twenty sixes of the events, approximately 86%, of these 35 events with various focal mechanisms are positive related to generate tsunamis or no tsunamis, where strike-slip earthquakes contribute 43% to tsunami excitation, and normal-earthquakes take a greater portion of 43%. The results suggest that, in terms of relative contribution, the slightly large portion given by the normal faults and the strike-slips earthquakes are ability to relate of tsunamis or no tsunamis.


## ACKNOWLEDGEMENTS

We firmly acknowledge GEOFON GFZ and Incorporated Research Institutions for Seismology (IRIS) for which seismic data were available from their respective sites at http://eida.gfz-potsdam.de/webdc3/ and http://www.iris.edu/wilber3/find. This work is funded by DRPM, The Ministry of Education and Culture, The Republic of Indonesia under grant number 217/SP2H/LT/DRPM/2021.


.

## REFERENCES


Carvajal, M., Araya-Cortejo, C., Sépulveda, I., Melnick, D. & Haase, J. S., 2019. Nearly instantaneous tsunamis following the $M_w$ 7.5 2018 Palu earthquake, *Geophys. Res. Lett.,* **46**, 1-33, doi:10.1029/2019GL082578

Geist, E. L. & Bilek, S. L., 2001. Effect of depth-dependent shear modulus on tsunami generation along subduction zones, *Geophys. Res. Lett.*, **28**(7), 1315-1318.

Goda, K., Mori, N., Yasuda, T., Prasetyo, A., Muhammad, A. & Tsujio, D., 2019. Cascading geological hazards and risks of the 2018 Sulawesi Indonesia earthquake and sensitivity analysis of tsunami inudation simulations, *Front. Earth Sci.*, **7**(261), doi:10.3389/feart.2019.00261.

Goldstein, P. & Snoke, A., 2005. SAC availability for the IRIS community. United States. *Incorporated Research Institutions for Seismology Newsletter* **7**(1).

Gusman, A. R., Satake, K., & Harada, T., 2017. Rupture process of the 2016 Wharton Basin strike‐slip faulting earthquake estimated from joint inversion of teleseismic and tsunami waveforms. *Geophys. Res. Lett.*, **44**, 4082-4089, doi:10.1002/2017GL073611.

Gusman, A. R., Supendi, P., Nugraha, A. D, Power, W., Latief, H., Sunendar, H., Widiyantoro, S., Daryono, Wiyono, S. H., Hakim, A., Muhari, A., Wang, X., Burbidge, D., Palgunadi, K., Hamling, I. & Daryono, M. R., 2019. Source model for the tsunami inside Palu Bay following the 2018 Palu earthquake, Indonesia. *Geophys. Res. Lett.*, **46**(15), 8721-8730, doi:10.1029/2019GL082717.

Heidarzadeh, M., Muhari, A. & Wijanarko, A. B., 2019. Insights on the source of the 28 September 2018 Sulawesi tsunami, Indonesia based on spectral analyses and numerical simulations. *Pure Appl. Geophys.*, **176**, 25-43, doi:10.1007/s00024-018-2065-9.

Imamura, F., Synolakis, C. E., Gica, E., Titov, V., Listanto, E. & Lee, H. J., 1995. Field survey of the 1994 Mindoro Island, Philippines tsunami. *Pure Appl. Geophys.*, **144**(3-4), 875-890, doi:10.1007/BF00874399.

Lay, T., Ye, L., Bai, Y., Cheung, K. F., & Kanamori, H., Freymueller, J., Steblov. G. M. & Kogan, M. G., 2017. Rupture along 400 km of the Bering fracture zone in the Komandorsky islands earthquake ($M_W$ 7.8) of 17 July 2017. *Geophys*. *Res*. *Lett*., **44**(12), 12161-12169, doi:10.1002/2017GL076148.

Lomax, A. & Michelini, A., 2009a. Mwpd: a duration-amplitude procedure for rapid determination of earthquake magnitude and tsunamigenic potential from *P*-waveforms, *Geophys. J. Int*., **176**, 200-214, doi:10.1111/j.1365-246X.2008.03974.x.

Lomax, A. & Michelini, A., 2009b. Tsunami early warning using earthquake rupture duration, *Geophys*. *Res*. *Lett*., **36**, L09306, doi:10.1029/2009GL037223.

Lomax, A. & Michelini, A., 2011. Tsunami early warning using earthquake rupture duration and *P*-wave dominant period: the importance of length and depth of faulting. *Geophys*. *J. Int*., **185**(1), 283-291.

Lomax, A. & Michelini, A., 2013. Tsunami early warning within five minutes. *Pure Appl. Geophys.,* **170**, 1385-1395, doi:10.1007/s00024-012-0512-6.

Ma, K-F., Satake, K. & Kanamori, H., 1991. The origin of the tsunami excited by the 1906 San Francisco earthquake, *Bull*. *Seismol*. *Soc*. *Am*., **81**(4), 1396-1397.

Madlazim, 2013. Assessment of tsunami generation potential through rapid analysis of seismic parameters-case study: comparison of the Sumatra earthquakes of 6 April and 25 October 2010, *Sci*. *Tsu*. *Hazards* **32**(1), 29-38.

Madlazim & Prastowo, T., 2016. Evaluation of earthquake parameters used in the Indonesian Tsunami Early Warning System, *Earthq*. *Sci*. **29**(1), doi:10.1007/s11589-016-0143-6.

Madlazim, Rohadi, S., Koesoema, S. & Meilianda, E., 2019. Development of tsunami early warning application four minutes after an earthquake. *Sci*. *Tsu*. *Hazards* **38**(3), 132-141.

Madlazim and Supriyono, 2014. Improving Experiment design skills: Using the Joko program as a learning tool of tsunami topic. *Sci. Tsu. Hazards*. **33**(2), 133-143

Madlazim, Prastowo, T., Fahmi, M.N. 2020. Estimation of Rupture Directivity, CMT And Earthquake Tsunami Parameters And Their Correlation with The Main Source of The First Tsunami Wave, September 28, 2018. Science of Tsunami Hazards . Nov2020, Vol. 39 Issue 4, p228-242. 15p.

Muhari, A., Imamura, F., Arikawa, T., Hakim, A., & Afriyanto, B., 2018. Solving the puzzle of the September 2018 Palu, Indonesia, tsunami mystery: clues from the tsunami waveform and the initial field survey data, *J. Disaster Res*., **13**, sc20181108, doi:10. 20965/jdr.2018.sc20181108.

Necmioglu, Ö. & Özel, N. M., 2014. An earthquake source sensitivity analysis for tsunami propagation in the eastern Mediterranean, *Oceanog*., **27**(2), 76-85, doi:10.5670/oceanog.2014.42.

Power, W., Clark, K., King, D. N., Borrero, J., Howarth, J. & Lane, E. M., 2017. Tsunami runup and tide-gauge observations from the 14 november 2016 M7.8 Kaikoura earthquake, New Zealand. *Pure Appl*. *Geophys*., **174**(7), 2457-2473.

Socquet, A., Hollingsworth, J., Pathier, E., & Bouchon, M., 2019. Evidence of supershear during the 2018 magnitude 7.5 Palu earthquake from space geodesy. *Nat*. *Geosci*., **12**, 192-199, doi:10.1038/s41561-018-0296-0.

Thatcher, W., Marshall, G. & Lisowski, M., 1997. Resolution of fault slip along the 470-km-long rupture of the great 1906 San Francisco earthquake and its implications, *J. Geophy*s. *Res*., **102**, B3, 5353-5367.

Ulrich, T., Gabriel, A. A., Ampuero, J. P. & Xu, W., 2019a. Dynamic viability of the 2016 Mw 7.8 Kaikoura earthquake cascade on weak crustal faults. *Nat*. *Commun*., **10**(1), 1213. doi:10.1038/s41467-019-09125-w.

Ulrich, T., Vater, S., Madden, E. H., Behrens, J., van Dinther, Y., van Zelst, I., Fielding, E. J., Liang, C. & Gabriel, A. A., 2019b. Coupled, physics-based modeling reveals earthquake displacements are critical to the 2018 Palu, Sulawesi Tsunami, *Pure Appl*. *Geophys*., **176**(32), 4069-4109, doi:10.1007/s00024-019-02290-5

Ward, S. N. 2011. *Encyclopedia of Solid Earth Geophysics: Tsunami.* Edited by Harsh K. Gupta. National Geophysical Research Institute (NGRI). Council 51 of Scientific and Industrial Research (CSIR). Springer Netherlands: Dordrecht, Netherlands, 1-1539. e-ISBN: 978-90-481-8702-7.

ISSN 8755-6839

SCIENCE OF TSUNAMI HAZARDS

Journal of Tsunami Society International

Volume 40 Number 2 2021

# TSUNAMI MITIGATION – ONLINE LEARNING EFFECTIVENESS BY USING OMBAK LEARNING MODEL

**Madlazim, Eko Hariyono, and Dyah Permata Sari**

Universitas Negeri Surabaya, INDONESIA
E-mail: madlazim@unesa.ac.id

## ABSTRACT

Many communities in Indonesia are potentially affected by tsunamis but do not have adequate preparedness in dealing with such disasters. This study aims to improve the preparedness capacity of the people living around the coast that are potentially affected by the tsunami through tsunami mitigation learning by using OMBAK learning model. The learning is done online to avoid the transmission of covid-19. Before the online learning begins, the student community is asked to work on the tsunami mitigation pre-test. The number of people living around the coast who took part in this learning was 62 people, ranging in age from 13 to 55 years old. Furthermore, students were briefed via a zoom meeting (synchronous) about the implementation of this online learning, especially relating on how to learn tsunami mitigation by using disaster mitigation video media. In this tsunami mitigation learning process, students are allowed to learn asynchronously. We also allow students to discuss tsunami mitigation materials through the WhatApp Group (WAG) during the learning process. After completing the learning process, students were asked to work on post-test questions. Based on the results of the percentage analysis on the learning implementation, it was found that the implementation of tsunami mitigation learning by using OMBAK learning model was carried out very well. In addition, based on the analysis of t-test and gain score from pre-test and post-test data, it was obtained that there was a significant increase in the students' tsunami mitigation ability.

***Keywords:*** *OMBAK learning model, online learning, tsunami mitigation capabilities, tsunami potential*

## 1. INTRODUCTION

Several areas in various parts of the country have the potential for a tsunami occurrence, but there are still many communities that are potentially affected by the tsunami that do not have the preparedness in dealing with a tsunami disaster. Therefore, learning about disaster mitigation that aims to improve their preparedness capabilities in dealing with a tsunami disaster that may come at any time is very important. Tsunami mitigation learning models that have been tested for their feasibility include the ORSAEV learning model (Madlazim et al., 2020; Madlazim, Supriyono, 2014), and the OMBAK learning model (Madlazim and Haryono, E., 2020; Sunarti, T. et al., 2018). In this study, the OMBAK learning model was used to improve community preparedness in dealing with the tsunami disaster because this learning model could be applied to online learning. This research is focused on people who live in East Java areas that are potentially affected by the tsunami; they are Trenggalek, Tulungagung, Blitar, Malang, and Pacitan Regency-Indonesia. This is based on the analysis results of the Meteorology, Climatology and Geophysics Agency (BMKG) in 2021 regarding the potential for a tsunami in East Java that the video can be accessed at the following link: http://bit.ly/VideoDaerahPotensiTsunami.

In general, disaster mitigation practices can be grouped into structural mitigation and non-structural mitigation. Structural mitigation is related to physical construction development efforts, while non-structural mitigation includes land use planning, enacting development regulations, and through education to prepare people to get used to live together with disasters, especially for environments that have already been built, so that people can feel the security and comfort in their life. (Rusilowati et al., 2012; Hariyono E. et al., 2016)). Disaster mitigation education can be done with various models or approaches in learning. Medias like posters, videos and comics are very suitable media in increasing students' understanding, especially disaster education materials. This is in accordance with Edgar Dale's theory about the cones of experience (https://en.wikipedia.org/wiki/Edgar_Dale#Cone_of_Experience). The cone of experience proposed by Edgar Dale illustrates that the learning experience can be obtained through the process of action or experiencing by us what is learned, the process of observing, and listening through certain media and the process of listening through language. This theory explains that the level of student involvement through verbal, visual, engaging and action approaches has a different effect on students' understanding and memory. The hope in the future is that the online learning will not be stopped and people are expected to have knowledge, skills, and positive attitudes in dealing with the tsunami disaster through integration in continuous learning from generation to generation so that a community with disaster education and awareness of disaster response will be created (Nugroho, A., 2019).

Learning in the 4.0 era requires more technology and information, especially in this era of the covid-19 pandemic that forces us to apply online learning. Tsunami mitigation learning cannot be carried out optimally because learning is carried out online so that some tsunami mitigation skills cannot be trained online to the maximum extent. In this study, we apply the OMBAK learning model to improve preparedness in dealing with tsunami disasters through online learning. The problem to be solved is how effective online learning on tsunami mitigation by using the OMBAK learning model is.

## 2. METHOD

The applied method in this research can be explained as follows. Learning is done online to avoid the transmission of covid-19. Before online learning begins, the student community is asked to work on the tsunami mitigation pre-test questions that can be accessed online at the following link https://forms.gle/8Ai4iaPMiX7eHeUWA. The number of people living around the coast who

participated in this study were 62 people ranging in age from 13 years to 55 years old. Furthermore, students were briefed via zoom meeting (synchronous) about the implementation of this online learning, especially those related to how to learn tsunami mitigation by using disaster mitigation video media. In this tsunami mitigation learning process, students are given the opportunity to learn asynchronously either independently or in groups. We also give students the opportunity to discuss tsunami mitigation materials through the WhatsApp Group (WAG) during the learning process. Students can ask questions or discuss with fellow students or with us as trainers.

In this learning process, the OMBAK learning model has been applied. Four phases in the OMBAK model learning, which are **Orientation, Understanding, Action, and Correction** (Madlazim and Hariyono, E., 2020) have been applied in this online learning. The orientation phase has been carried out synchronously by the trainer through a zoom meeting. In the understanding phase, students have been given the opportunity to learn either independently or in groups, either synchronously or asynchronously, and in a reasonable time. Students are also given tsunami mitigation video media to be studied online and can be accessed at the link: https://drive.google.com/drive/folders/14pRBXZuKAZvAp17wvELF3N0YQoy4xrpw?usp=sharing .

The action phase can be trained independently by students after watching the tsunami mitigation video. In this correction phase, participants can correct the training stages that have been carried out and recorded and then compared with the training stages available in the video. Furthermore, this correction phase is also carried out by the trainer on the video recording that has been done by the students. After completing the learning process, students are asked to work on post-test questions which can be accessed online at the following link http://bit.ly/PostMitigasiTsunami.

This learning implementation sheet was observed and assessed by two observers consisting of a learning expert and a practitioner (lecturer) who used the percentage criteria of learning implementation (PK) (Yamansari, 2010). Percentage criteria PK < 50% (not good), 50%≤*PK*<70%2 (good enough), 70%≤*PK*<85% (good), and *PK*≥85% (very good). The pretest and posttest data were then analyzed for the significance of the difference by using t-test and the increase by using a gain score (Hake, 1999). Observational data in the form of percentage criteria of learning implementation (PK) were analyzed by Yamansari criteria (2010).

## 3. RESULTS AND DISCUSSION

The results of this study are in the form of solutions whether online learning on tsunami disaster mitigation that applies OMBAK learning model is carried out well or not and effective or not. To answer these problems, pre-test, post-test data and observational data on the learning implementation are needed for each phase of the OMBAK learning model, from all the domain of knowledge, skills and attitudes towards tsunami mitigation preparedness. The results of the N-gain score analysis are shown in Table 1.

**Table 1**. Results of N-Gain Score Analysis for Attitudes, Knowledge and Skills of Tsunami Mitigation

| No | Name | N-Gain Score | | |
|---|---|---|---|---|
| | | ATTITTUDE | KNOWLEDGE | SKILL |
| 1 | Respondent 1 | 0.38 | 1.00 | 0.67 |
| 2 | Respondent 2 | 1.00 | 1.00 | 0.50 |
| 3 | Respondent 3 | 0.80 | 0.50 | 0.67 |
| 4 | Respondent 4 | 0.25 | 0.50 | 0.25 |

| | | | | |
|---|---|---|---|---|
| 5 | Respondent 5 | 0.50 | 0.60 | 0.67 |
| 6 | Respondent 6 | 0.67 | 0.33 | 0.67 |
| 7 | Respondent 7 | 0.67 | 0.67 | 0.25 |
| 8 | Respondent 8 | 0.33 | 0.20 | 0.50 |
| 9 | Respondent 9 | 0.22 | 0.67 | 0.67 |
| 10 | Respondent 10 | 0.67 | 0.50 | 0.75 |
| 11 | Respondent 11 | 0.36 | 0.67 | 0.00 |
| 12 | Respondent 12 | 0.25 | 1.00 | 1.00 |
| 13 | Respondent 13 | 0.67 | 1.00 | 0.67 |
| 14 | Respondent 14 | 0.25 | 1.00 | 0.33 |
| 15 | Respondent 15 | 0.50 | 1.00 | 0.33 |
| 16 | Respondent 16 | 0.67 | 1.00 | 0.00 |
| 17 | Respondent 17 | 0.75 | 0.50 | 0.67 |
| 18 | Respondent 18 | 0.50 | 0.75 | 0.50 |
| 19 | Respondent 19 | 0.40 | 0.33 | 0.50 |
| 20 | Respondent 20 | 0.67 | 1.00 | 0.50 |
| 21 | Respondent 21 | 0.50 | 1.00 | 0.33 |
| 22 | Respondent 22 | 0.50 | 0.75 | 0.67 |
| 23 | Respondent 23 | 0.60 | 1.00 | 0.50 |
| 24 | Respondent 24 | 0.30 | 0.67 | 1.00 |
| 25 | Respondent 25 | 0.67 | 0.75 | 0.60 |
| 26 | Respondent 26 | 0.70 | 1.00 | 1.00 |
| 27 | Respondent 27 | 0.67 | 1.00 | 0.50 |
| 28 | Respondent 28 | 0.33 | 0.75 | 0.50 |
| 29 | Respondent 29 | 0.67 | 0.75 | 0.67 |
| 30 | Respondent 30 | 0.50 | 0.50 | 0.67 |
| 31 | Respondent 31 | 0.75 | 0.33 | 0.50 |
| 32 | Respondent 32 | 0.40 | 0.50 | 1.00 |
| 33 | Respondent 33 | 0.43 | 0.67 | 0.60 |
| 34 | Respondent 34 | 0.75 | 1.00 | 0.33 |
| 35 | Respondent 35 | 0.43 | 1.00 | 0.50 |
| 36 | Respondent 36 | 0.33 | 0.75 | 1.00 |
| 37 | Respondent 37 | 0.30 | 0.50 | 0.67 |
| 38 | Respondent 38 | 0.67 | 0.75 | 0.00 |
| 39 | Respondent 39 | 0.25 | 1.00 | 1.00 |
| 40 | Respondent 40 | 0.30 | 0.67 | 0.67 |
| 41 | Respondent 41 | 0.20 | 1.00 | 1.00 |
| 42 | Respondent 42 | 1.00 | 1.00 | 1.00 |
| 43 | Respondent 43 | 0.75 | 0.50 | 0.50 |
| 44 | Respondent 44 | 0.56 | 0.80 | 0.75 |
| 45 | Respondent 45 | 0.30 | 0.25 | 0.33 |
| 46 | Respondent 46 | 0.22 | 1.00 | 1.00 |
| 47 | Respondent 47 | 0.67 | 0.67 | 0.50 |
| 48 | Respondent 48 | 0.50 | 0.67 | 1.00 |
| 49 | Respondent 49 | 0.33 | 0.75 | 0.75 |
| 50 | Respondent 50 | 0.70 | 0.67 | 1.00 |
| 51 | Respondent 51 | 0.50 | 0.33 | 0.75 |

| | | | | |
|---|---|---|---|---|
| 52 | Respondent 52 | 0.70 | 0.75 | 1.00 |
| 53 | Respondent 53 | 0.75 | 0.67 | 0.25 |
| 54 | Respondent 54 | 0.25 | 1.00 | 0.67 |
| 55 | Respondent 55 | 0.25 | 0.33 | 0.50 |
| 56 | Respondent 56 | 0.33 | 0.67 | 0.67 |
| 57 | Respondent 57 | 0.67 | 0.33 | 0.50 |
| 58 | Respondent 58 | 0.67 | 0.50 | 0.67 |
| 59 | Respondent 59 | 0.33 | 0.67 | 1.00 |
| 60 | Respondent 60 | 0.67 | 1.00 | 0.67 |
| 61 | Respondent 61 | 0.42 | 0.67 | 1.00 |
| 62 | Respondent 62 | 0.75 | 0.50 | 0.67 |
| Total | | 32.08 | 44.27 | 38.97 |
| Average | | 0.52 | 0.71 | 0.63 |
| Category | | MEDIUM | HIGH | MEDIUM |

The ability of tsunami disaster mitigation in the attitude aspect was measured by using a tsunami disaster mitigation attitude test in the form of a questionnaire consisting of 10 attitude statements, both positive and negative statements with four answer choices adopted by using a Likert scale. The level of tsunami disaster mitigation capability in the aspect of community attitudes towards tsunami mitigation increased to the moderate category (Table 1). The increase in the attitude aspect of tsunami mitigation is the lowest compared to the increase in the aspect of knowledge, and skills because to improve this attitude aspect, it requires habituation in the practice of daily life repeatedly and continuously and also requires an example. This thing cannot be fully obtained through online learning. The results obtained from observing the implementation of online learning on tsunami mitigation are used as an indicator of the researchers' success in carrying out each phase of the OMBAK learning model. The results of the observations are shown in Table 2 below:

**Table 2.** Recapitulation of Learning Implementation of OMBAK Learning Model

| Activities of Each Phase | Score | Criteria |
|---|---|---|
| **Orientation (Synchronos)** | 89% | Very Good |
| **Understanding** (Understanding the concept/knowledge of tsunami mitigation) (Asynchronos) | 87% | Very Good |
| **Action (Asynchronos)** | 78% | Good |
| **Correction (Combination of synchronos and Asynchronos)** | 86% | Very Good |
| **Average** | 85 | Very Good |

The main strategy in the disaster learning process is learning by doing. Based on these considerations, the learning strategy is carried out with conceptual learning at an early stage, and then followed by practical learning, and it is hoped that the community will have a strong attitude in dealing with the tsunami disaster. Conceptual learning is carried out to provide basic knowledge about tsunami disasters. This basic knowledge of tsunami disaster includes knowledge of the potential tsunami disaster threat, vulnerability, capacity, and tsunami disaster risk. Practical learning is carried out with the aim that the community can have skills in tsunami disasters, which include

preparedness, emergency, and recovery exercises, as well as preparing disaster management plans and contingency plans both independently and in groups. The outcome of the tsunami disaster learning process followed by the community was the profile of the community with an insight into tsunami disaster risk reduction (Munadi et al., 2019). Habituation is a process of forming attitudes and behaviors that are relatively permanent and automatic through a repetitive

learning process. Attitudes or behaviors that become habits have characteristics; The behavior is relatively permanent, generally does not require a high enough thinking function, for example, to be able to say greetings, the thinking function is in the form of remembering or imitating only, not as a result of the maturity process, but as a result of experience or learning, and appears repeatedly. in response to the same stimulus (Amirulloh, Syarbini, 2012).

The learning outcomes of tsunami mitigation knowledge aspects are measured by using a tsunami disaster mitigation knowledge test in the form of multiple-choice questions consisting of 10 items. The learning outcomes of tsunami mitigation knowledge aspects experienced the highest increase in online learning by using the OMBAK learning model and based on the results of the gain score analysis as shown in Table 1, it was in a high category, but still not optimal because the control in online learning carried out by the community was very weak, so it is very possible for people who do not have high learning motivation, that they learn not optimally. For for the results of this online learning to be optimal, the instructor needs to implement a more stringent online learning control system. However, motivation is not enough, people must be able to manage time well. As a reference, people can imitate the Pomodoro technique, namely: 1. Make a list of tasks that must be done. 2. Do the task for 25 minutes. 3. Check the list of completed tasks. 4. Rest for 5 minutes. 5. Back to study for 25 minutes + 5 minutes rest. This is a Pomodoro activity. 6. After carrying out 4 Pomodoro activities, take a long break of about 30 minutes (Shinoda, K., 2020).

The learning outcomes of the tsunami mitigation skills aspect were measured by using a tsunami disaster mitigation skills test in the form of multiple-choice questions consisting of 10 items. The learning outcomes for tsunami mitigation skills in this study reached the medium improvement category. Although the increase in tsunami mitigation skills in this study did not reach the high category, in online learning this achievement was classified as effective. Piaget argues that learning interactions in the aspects of knowledge, skills and attitudes take place continuously, which are carried out by individuals with their environment, while the environment itself is constantly changing. With the change in the environment, it means that the learning function is constantly evolving. Hamalik, U. (2001) defines learning as a systematically arranged combination of humans, materials, facilities, equipment and procedures, to achieve learning objectives. Humans involved in learning include teachers, students and administration, materials in the form of books, blackboards, photos, videos and audiovisuals. Procedures include schedules and methods of delivering information including learning models, practices, exams, and so on. In this online lesson, the ability of tsunami mitigation skills can be improved through the examples provided in 4 tsunami mitigation videos. Furthermore, people imitate as in the video.

## 4. CONCLUSIONS

The implementation of online learning on the topic of tsunami mitigation by using the OMBAK learning model has very good criteria and can significantly increase the ability of tsunami mitigation preparedness. This learning has made students have the ability to prepare for tsunami mitigation, in the domain of knowledge, skills, and attitudes of students towards tsunami mitigation preparedness. They are also more enthusiastic and actively involved in the learning process even though it is carried out online. This can be seen from the number of questions submitted via the WA group. Based on this study results, it can be conveyed that OMBAK becomes an effective learning media of tsunami lessons for coastal communities in dealing with tsunami disasters, especially in the pandemic era.

**ACNOWLEDGMENTS**

Our gratitude goes to the Research and Community Service Council (DRPM) of the Directorate General of Higher Education contract no. 045/SP2H/LT/DRPM/2021 and contract no. SPK B/12090/UN38.9/LK.04.00/2021.

**REFERENCES**

Amirulloh, Syarbini (2012). *Buku Pintar Pendidikan Karakter*. Jakarta: as@-Prima Pustaka.

Edgar Dale, https://en.wikipedia.org/wiki/Edgar_Dale#Cone_of_Experience. Accessed on 17 June 2021.

Hake, R. R. (1999). *Analyzing change/gain score*. [Online] Tersedia: http://www.physics.indiana.edu/nsdi/AnalyzingChange-Gain.pdf [Diakses 3 Januari 2017].

Hamalik, Oemar. 2001. Proses Belajar Mengajar. Jakarta: PT. Bumi Aksara.

Hariyono, E., Liliasari, L., Tjasyono, B., Madlazim, M. (2016). Volcanic eruption crisis and the challenges of geosciences education in Indonesia. *AIP Conference Proceedings 1708*.

Madlazim, Rahmadiarti, F., Masriyah, Indana, S., Sunarti, T., & Prahani, B. K. (2020). An OrSAEv learning model to improve the disaster preparedness of STEM teacher candidates. *World Transactions on Engineering and Technology Education*, *18*(2), 231–236.

Madlazim, Supriyono (2014). Improving experiment design skills: Using the Joko Tingkir program as a learning tool of Tsunami topic. *Science of Tsunami Hazards* 33(2), pp. 133-143

Madlazim and Haryono E. (2020). Mechanism of Increasing Preparedness Tsunami: Ombak - Learning Model Development. *Science of Tsunami Hazards, 39(3), 156-167.*

Paripurno, Munadi, Koesuma, Ismail, & Mardiatmo, 2019. Panduan Pembelajaran Kebencanaan Untuk Mahasiswa Di Perguruan Tinggi. Direktorat Jenderal Pembelajaran Dan Kemahasiswaan Kementerian Riset Teknologi Dan Pendidikan Tinggi.

Nugroho, Agung. Model Pembelajaran Mitigasi Bencana Tsunami. Di Sekolah Dasar Pesisir Pantai Selatan Jawa *Prosiding Seminar Nasional Diselenggarakan Pendidikan Geografi Fkip Ump. "Manajemen Bencana Di Era Revolusi Industri 5.0". Isbn 978-602-6697-38-7. Purwokerto, 10 Agustus 2019.*

Rusilowati, A. 2012. Mitigasi Bencana Alam Berbasis Pembelajaran Bervisi Science Environment Technology And Society. *Jurnal Pendidikan Fisika Indonesia Januari 2018.*

Shinoda, K., 2020. Pomodoro Technique For Improving Students' Reading Ability During Covid-19 Pandemic. DOI: 10.37081/ed.v8i3.1753

Sunarti, T., Prahani, B.K., Wasis, Madlazim, Suyidno (2018). Effectiveness of CPI(Construction, production, and implementation) teaching model to improve science literation for pre-service physics teacher). *Journal of Science Education* 19(1), pp. 73-89.

Yamansari, Y. (2010). Pengembangan Media Pembelajaran Matematika Berbasis ICT yang Berkualitas. *Seminar Nasional Pascasarjana X-ITS, Surabaya.* Agustus 2010 (2-8).

ISSN 8755-6839

SCIENCE OF TSUNAMI HAZARDS

Journal of Tsunami Society International

Volume 40 Number 2 2021

# THE GREAT TANGSHAN EARTHQUAKE OF 28 JULY 1976 IN CHINA - Analysis of Tsunami Generation in the Bohai and Yellow Seas

**George Pararas-Carayannis**

Tsunami Society International

## ABSTRACT

No other earthquake in the 20th or 21st centuries was as catastrophic or claimed as many lives as that which struck the city of Tangshan in Northern China on 28 July 1976. Tangshan, a thriving industrial city of 1.6 million people in the Province of Hebei is located about 95 miles east and slightly south of Beijing and about 280 miles southwest of Haicheng of Liaoning Province. The main magnitude 7.8 earthquake was followed some 15 hours later by a 7.1 magnitude major event and numerous aftershocks. The first two events were mainly responsible for the destruction or severe damage of 93 percent of unreinforced houses, multistory residential buildings, and other structures in Tangshan and its southern suburb along the Beijing-Shanhaiguan railway. According to government records, the earthquake killed 242,769 people and severely injured another 169,851. However, based on the density of the population and the extent of the destruction, these figures have been disputed. The death toll has been estimated to have been three times greater than reported. The present study reviews the seismotectonics of the region, the aftershock distribution, the strike-slip ground motions of major existing faults along the YanShan and the Cangdong fold-fault zones, the Shanxi fault depression structural belt, the Taihang piedmont fault zone, the Guangdong and Tangcheng-Lijiang fault zones and the 1976 TangShan earthquake's intensities and ground motions, as well as the downward tilting and crustal displacements of sedimentary layers along the coasts of Bohai Bay**.** Based on this review and analysis, the present study examines the reasons why only a small tsunami was generated in Bohai Bay, even though earthquake intensities were high, ranging from VI to VIII.

***Keywords:*** *Tangshan earthquake, Liaoning Province seismicity, YanShan Cangdong fold-fault zones, Shanxi structural belt, Taihang Piedmont fault zone, Bohai Sea tsunamis*

## 1. INTRODUCTION

Tangshan is a major city in the Hebei Province of China bordering Bohai Bay and Sea in the upper Yellow Sea. Two earthquakes on July 28, 1976, in the Hebei Province of northeastern China struck and totally destroyed the city of Tangshan – a city of 1.6 million inhabitants (Pararas-Carayannis, 2007; 2008a). The main quake had a magnitude of M 7.8 and an epicenter at 39.4 N. 118.0 E. (Fig. 1). It was followed by a major 7.1 magnitude destructive aftershock, some 15 hours later, that had a magnitude of M 7.1. The earthquake took a heavy toll on infrastructure and agriculture. Although not adequately documented, given the intensities of ground motions near the coast, a small tsunami was generated in the Bohai Bay of the Yellow Sea.

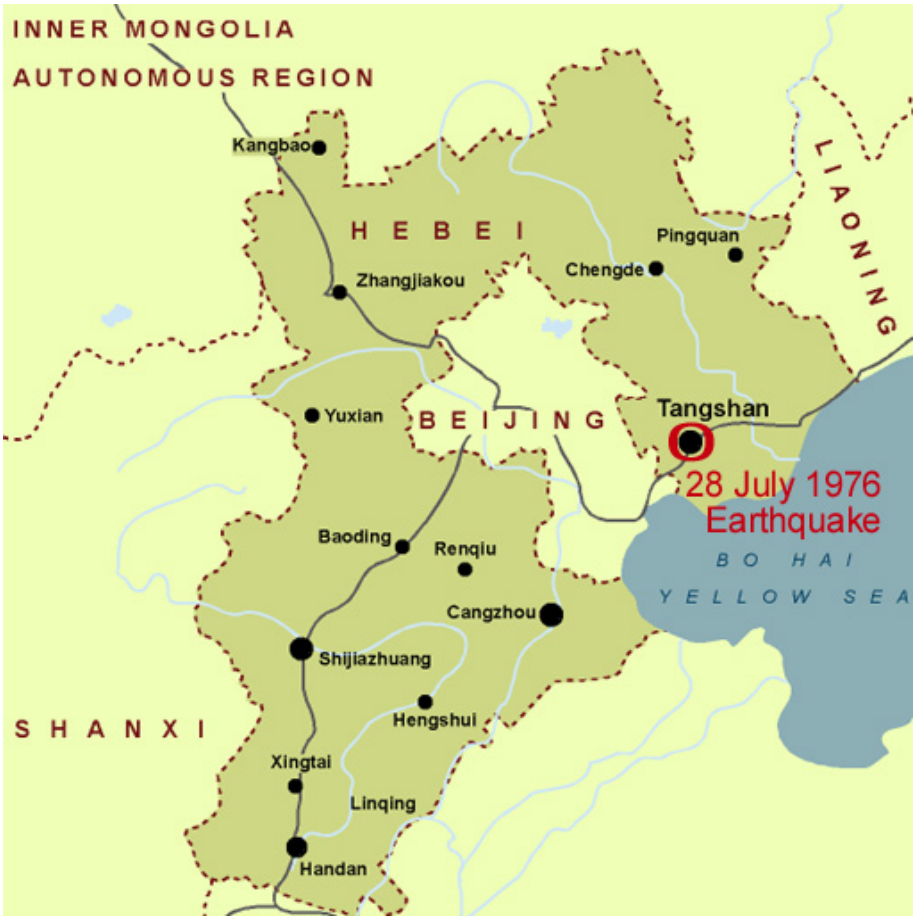


*Fig. 1. Epicenter of the Tangshan Earthquake of 28 July 1976 in the Hebei Province of* Both events were shallow (15 km) and occurred near the coast of Bohai Bay. *China.*

There were no foreshocks or clear precursory phenomena prior to the Tangshan earthquake - as there had been in other earthquake-stricken areas of China. However,

half a month earlier there had been a series of abnormal signals observed in the regions of Beijing, Tianjin, Tangshan, Bohai and Zhangjiakou. Also, just prior to the earthquake, many unusual phenomena were observed in the immediate Tangshan region. There were observations of large amplitude variations of groundwater level and of strange animal behavior - – indicating that something was going to happen.

As early as July 12, it was reported that gas began to discharge from a well in a village. On July 25 and 26, this discharge increased. The day before the earthquake, well water at another village reportedly rose and fell three times and other wells showed signs of cracking of their lining. The night before the earthquake, many people in Tangshan reported seeing strange lights in the sky and hearing loud sounds. Some people reported seeing lights of multiple hues and fireballs traversing the skies. Unfortunately, these were isolated incidents that were spread over a large area in a heavily populated region of China, thus no special significance was given at the time. The anomalous precursory phenomena were widely scattered and inconclusive. They occurred too late to be of usefulness for short-term prediction and warning purposes. The only community that paid attention to the precursory phenomena was that of Qinglong County. Special emergency meetings for preparedness were held in the three days just prior to the earthquake – and this may have contributed to the greater survival rate in this County. Based on such signals the State Seismological Bureau had correctly concluded that a significant earthquake could be expected between July 22, 1976, and August 5. However, the precursory phenomena differed from those of other earthquakes. Because of the scattered distribution of the signals, there was no determination of the location where this earthquake would strike.

The following sections present more details on the Tangshan eartquake of 29 July 1976, on their aftershock distribution, earthquake's intensities, and ground motions, on the downward tilting and crustal displacements of sedimentary layers along the coasts of Bohai Bay, on the seismotectonics of the region, the strike-slip ground motions of major existing faults along the YanShan and the Cangdong fold-fault zones, the Shanxi fault depression structural belt, the Taihang piedmont fault zone, the Guangdong and the Tangcheng-Lijiang fault zones**,** as well as on the downward tilting and crustal displacements of sedimentary layers along the coasts of Bohai Bay and Sea**.** Based on this review and analysis, the present study examines the reasons why only a small tsunami was generated in Bohai Bay and Sea, even though the earthquake intensities were high.

## 2. THE GREAT TANGSHAN EARTHQUAKE OF 28 JULY 1976 IN NORTHERN CHINA

The great Tangshan earthquake with magnitude M 7.8 (later revised to moment magnitude Mw 7.6) and focal depth of 15 km occurred on July 28, 1976, at 19:42:53.8 UTC (local date and time: July 28, 1976, 03:42) in the Hebei Province of northeastern China. Its epicenter was at 39.60° N 118.20° E39.4 near the coast of the Bohai Sea (Fig. 1). The earthquake was felt in fourteen provinces of China, and as far as Xian, about 470 miles (756 km) away, in Beijing (about 140 km to the west), and in Tientsin (60 miles to the

southwest). Fifteen hours later, it was followed by a major 7.1 magnitude destructive aftershock in the Northeast, with an M 7.1 magnitude and epicenter at 39.7 N., 118.5 E. (Wang 1976; Mei, 1982; Yong et al 1988; Pararas-Carayannis, 2008a). Ground intensities in the area ranged from VI to VIII. Both events were shallow (15 km). Many strong aftershocks followed the larger earthquakes, two of which had magnitudes of 6.0 or more. In the following days, there were many more aftershocks ranging in magnitude from 5 to 5.5 (Fig. 2). Several months later, on 15 Nov 1976, a magnitude 6.0 earthquake struck again in the same region (Pararas-Carayannis, 2008c).

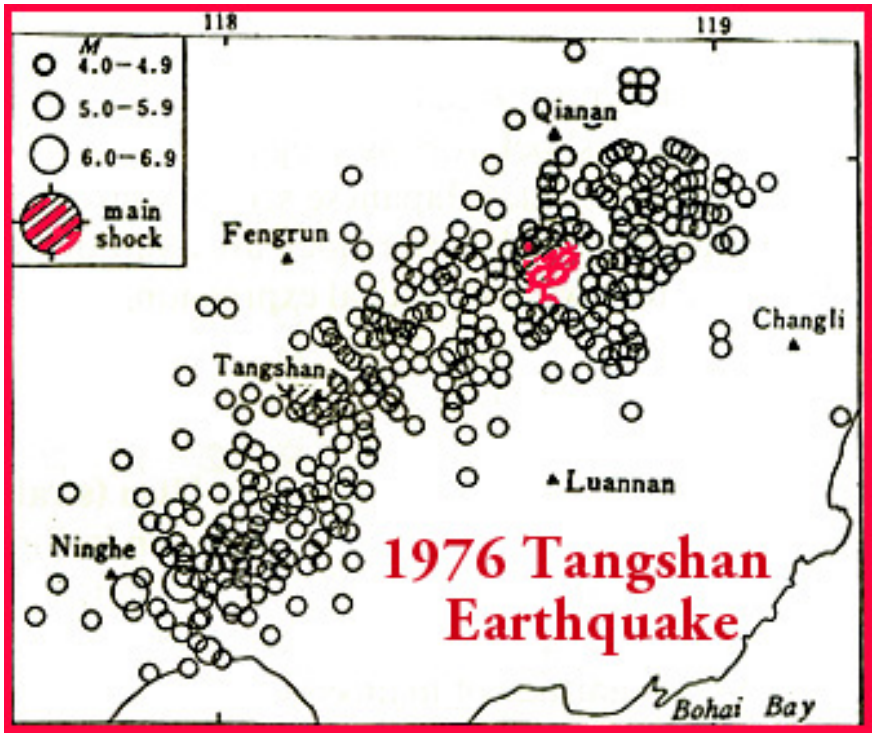


Fig. 2. The Epicenter and major aftershocks of the Earthquake of July 28, 1976 near Tangshan.

Figure 3 below is an aerial photo of Tangshan showing the degree of almost total destruction. According to local government accounts the 1976 earthquakes killed 242,769 people and severely injured another 169,851. However, based on the density of the population in the area and the fact that the earthquake destroyed ninety three percent of all residential buildings, the death toll was estimated to be three times greater than what had been reported, and to have ranged from 655,000 to 779,000 people.

The earthquake struck at 3:42 a.m. when most people were at home asleep. The timing contributed to the great death toll. What made matters worse, was the fact that the city of Tangshan is located in the center of an area surrounded with major

faults. Most of the structures in the region were extremely vulnerable because they had been built on unstable, alluvial soils. Consequently most these structures were destroyed. Only a few of the city's structures and building were earthquake-resistant but even the well built structures suffered serious damage.

*Fig. 3. Aerial photo of a section of Tangshan showing degree of destruction*

The zone of maximum destruction was estimated to be is about 47 square kilometers. It included the city of Tangshan and the southern suburb along the Beijing-Shanhaiguan railway. The earthquake's destruction was beyond description. Over a four-by-five mile area the devastation of the city was nearly total. Everything was completely leveled. About ninety-three percent of residential buildings and seventy-eight percent of commercial and industrial buildings in Tangshan were destroyed. Highway bridges and at least two dams collapsed. All roads, except for one were closed. Rails were bent causing the derailment of seven commercial trains. Homes and factories were leveled to the ground. There was a total destruction of the region's infrastructure. Electric power, water supply and sewer systems failed. All telephone and radio communications systems stopped functioning. Almost all of the irrigation wells became inoperative. Sand and water gushed from the ground and spread over large tracts of farmland. Mud volcanoes of up to 3 meters in diameter sprung up.

What made matters worse, was the fact that the city of Tangshan is located in the center of an area surrounded by major faults. Most of the structures in the region were extremely vulnerable because they had been built on unstable, alluvial soils. Consequently

-ost of these structures were destroyed. Only a few of the city's structures and buildings were earthquake-resistant but even the well-built structures suffered serious damage. The damage was not restricted to the Tangshan region only. Damage was reported from as far away as Qinhuangdao, Tianjin, and Beijing.

### 2.1 Earthquake Intensities and Ground Motions

There were substantial ground movements along the segment of the fault that ruptured. Along the west side, the ground moved laterally for about five feet (1.5m.), in a north/northeast direction sub-parallel to the major axis of the microseismic zone. However, in some areas, horizontal ground displacements of up to 7 meters were subsequently measured. On the eastern side of the rupture, the ground block tipped upward near the south end and downward at the northern end.

The intensities of the 1976 earthquake and its ground motions were extensively surveyed and reported (Figure 3). In the epicenter area, the intensity was estimated at XI (State Seismological Bureau). The region with intensity X was reported as being elliptical in shape, and covering a total area of about 370 km2. According to eyewitness reports, the shaking lasted for about 90 seconds. Ground motions were so strong that people reportedly were thrown in the air. The region of intensity of IX was reported as being rhombic in shape, trending in a northeast direction and covering an area of about 1,800 $km^2$. In this area, most of the homes were damaged and about 40 percent of them collapsed. The region of the,intensity VIII extended in a southeastward direction, and covered an area of about 7,300 $km^2$. The region of intensity VII was reported to cover an area of about 33,000 $km^2$.

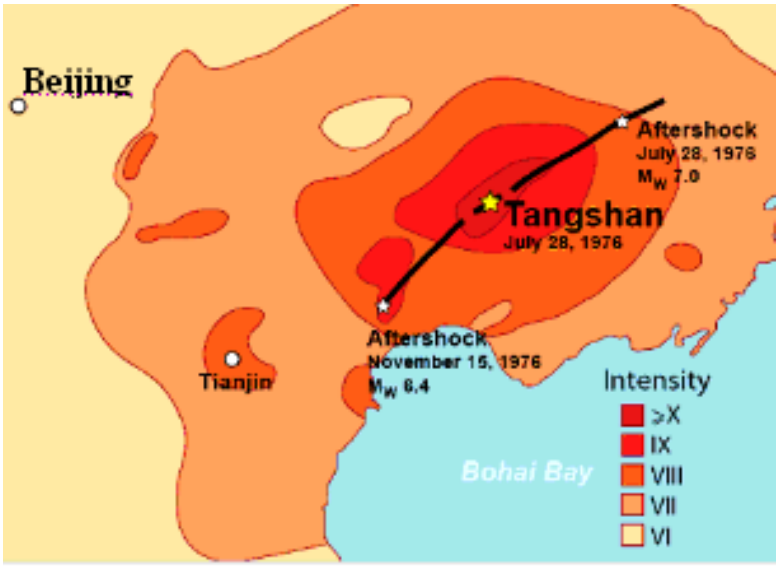


*Fig. 4. Map of intensities of the earthquake in Tangshan and surrounding areas bordering Bohai Bay (after Wang Fang 1976, State Seismological Bureau of China)*

The zone of maximum destruction was estimated to be about 47 $km^2$. It included the city of Tangshan and the southern suburb along the Beijing-Shanhaiguan railway. Over a four-by-five mile area, the devastation of the city was nearly total. About ninety-three percent of residential buildings and seventy-eight percent of commercial and industrial buildings in Tangshan were destroyed.

**2.2 Loss of Life and Damages**

The actual death toll from this earthquake may never be known with certainty. According to official government accounts the earthquake killed 242,769 people and severely injured another 169,851. However, based on the density of the population and the extent of the destruction, these figures have been disputed. As mentioned, Tangshan was a city with 1.6 million people. Combined the two earthquakes of 28 July 1976 destroyed ninety three percent of all residential buildings, and the death toll was estimated to be three times greater than what was reported - ranging from 655,000 to 779,000 people. At least 700,000 more people. At least 700,000 more people were injured, and property damage was extensive, reaching even Beijing. The extremely high death toll makes the 1976 Tangshan event the second worse earthquake disaster in recorded history. The most destructive earthquake ever occurred four centuries earlier in 1556 in Shaanxi, China. It is estimated that the 1556 earthquake killed 830,000 people. Another earthquake in the Gansu region in 1920 had killed about 200,000.

**2.3 Tsunami Generation in the Bohai and Yellow Seas**

Given the high intensities of the earthquakes near the coasts of Bohai Bay and Sea, a tsunami was generated and must have been responsible for deaths and damages. However, the devastation from the earthquake was so great, that no distinction was made of the effects of the tsunami in Bohai Bay and Sea or further away in the Yellow Sea. Figure 5 indicates earthquake intensities of VI, VII, and VIII along Bohai Sea's coastal region and the postulated source area of tsunami generation, even though crustal movements were predominantly of the strike-slip type, although the ground block tipped upward near the south end, thus contributing to tsunami generation.

Subsequent sections 3, 4, and 5 of the present report examine the neotectonics of the Bohai basin region, the impact of past historical events, and the postulated tsunami generated by the Great Tangshan earthquake of 28 July 1976, as indicated by the upward tipping of the southern ground block and the lateral compressive motions on consolidated sedimentary layers. Based on a previous analysis of the unique conditions of the Bohai Basin (Pararas-Carayannis, 2009), the present study examines and re-evaluates the potential for local tsunami generation from a variety of direct and collateral source mechanisms triggered by intraplate earthquakes such as the Tangshan event in the northeast region of China (Pararas-Carayannis http://tsunamisociety.org/281GPCC.pdf

More specifically, section 5 of the present study examines such collateral mechanisms of tsunami generation by the folding and en-echelon bookshelf failures of the consolidated sedimentary formations near the coasts of the Bohai Sea, as well as the very possible earthquake impact on the destabilization/dissociation of existing structural accumulations of gas hydrate deposits within the basin's thick, sedimentary stratigraphic layers. In brief, the potential for tsunami generation in the Bohai Sea was exacerbated by the thick accumulation of sediments (in different states of consolidation) and the multi-layered stratigraphic distribution of sediments with different shear strengths, densities, and rigidities. Following an earthquake, en-echelon, bookshelf type of failures occur with oblique directivity to the general strike orientation could impart greater tsunami energy and alter tsunami directivity. Thus, any mathematical modeling study must consider such complexities of source inputs for such environments of extreme sedimentation.

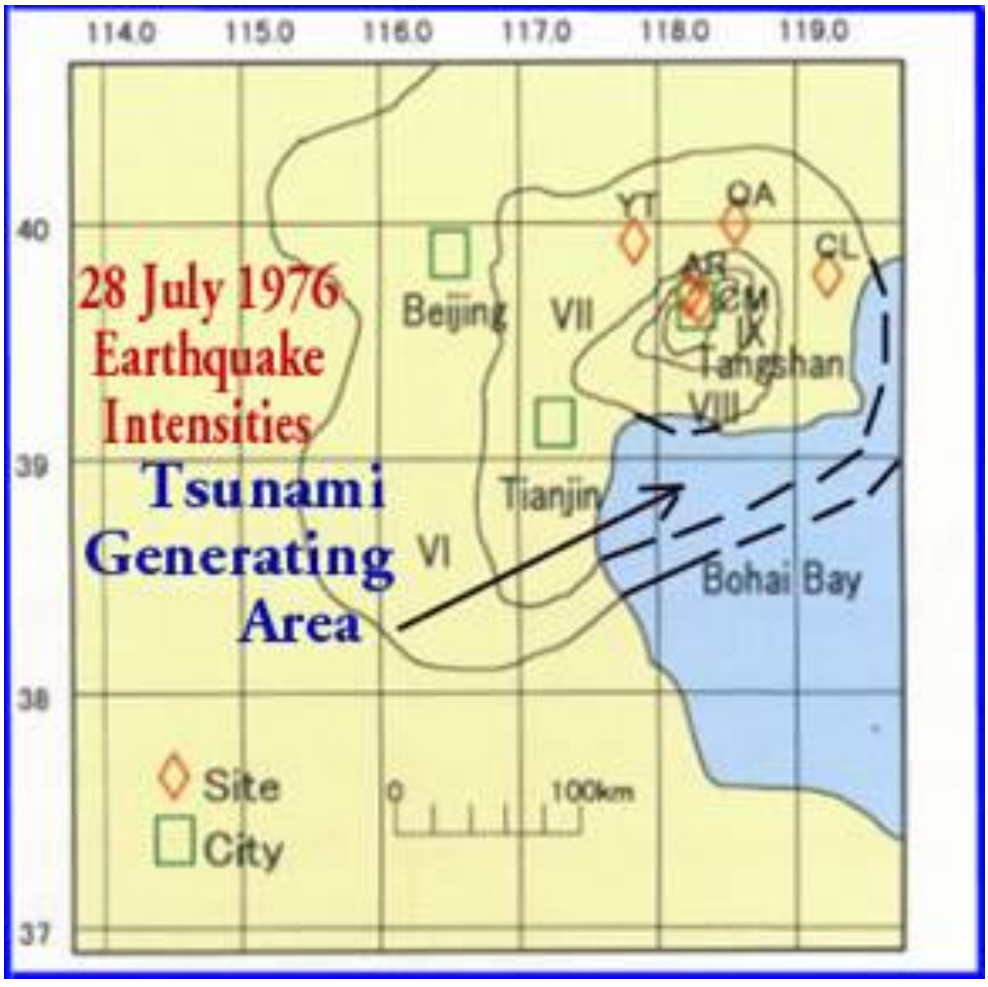


*Fig. 5. Intensities of Ground Motions of the Tangshan Earthquake (after Wang Fang 1976, State Seismological Bureau of China). Postulated Tsunami Generating Area.*

## 3.0 SEISMOTECTONICS OF THE TANGSHAN AREA AND OF NORTHERN CHINA

The high seismicity of central and eastern Asia results from the northward collision convergence (at about 50 mm/y) of the India tectonic plate against the Eurasian plate. This active collision - which begun about 55 million years ago during the Cenozoic era (Zhang et al, 1984; Hellinger et al 1985; Ye et al 1985; Yu et al 1995; Xu et al. 1996; Yin and Nie, 1996; Hendrix & Davis, 2001; Castellanos & Mann 2005; Zhao et al, 2005; Pararas-Carayannis, 2007; 2008; 2008b; 2008c; 2008d; 2009) - is the cause of frequent large earthquakes between India and Tibet, throughout Tibet and China. The convergence has uplifted the Asian highlands and the Tibetan Plateau to an average elevation of over 16,000 feet (about 4,880 meters) - the highest and largest plateau on Earth - with hundreds of kilometers of displacement of crustal blocks to the east and southeast in the direction of China. Thus, the high seismicity of China is dominated by this northward collision and convergence (Fig. 7).

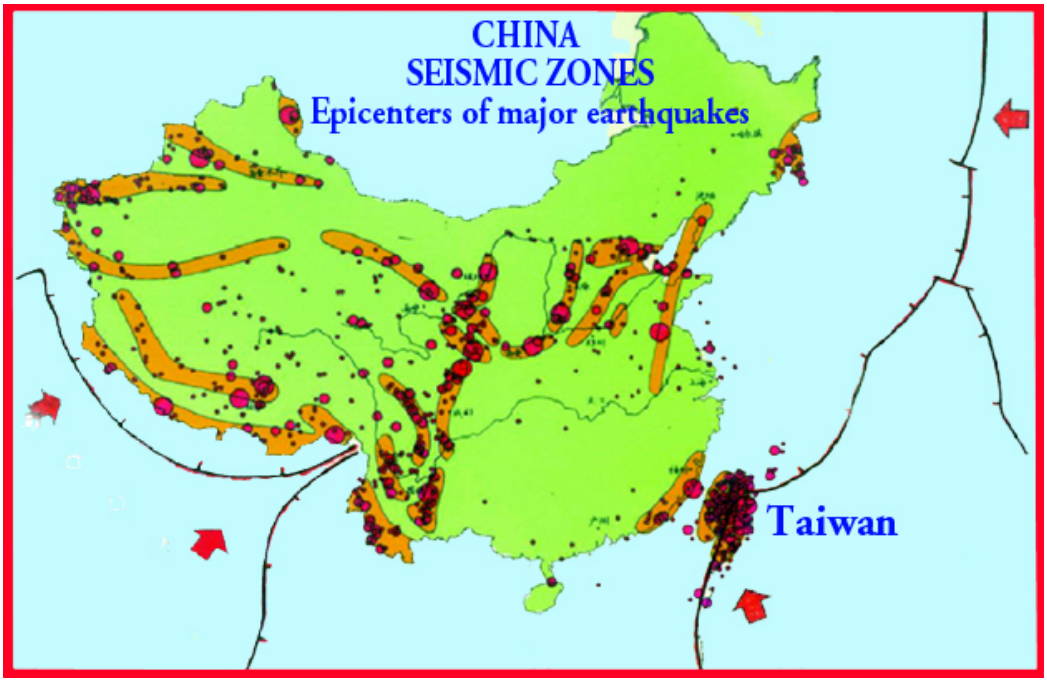


Fig. 7. China's Seismic Zones created by collision and convergence (after Pararas-Carayannis, 2007)

The active collision has resulted in three distinct deformational episodes in China that occurred 200-240 million years ago and resulted in initial thrusting and subsequent vertical extrusion, while later episodes resulted in folding (Li et al. 2007). The convergence has formed the most active and extensive seismic belts in China as shown in Fig. 7, and in the formation of major fault zones. Such crustal displacements along China's seismic zones are responsible for the large destructive earthquakes, which occur with high frequency.

### 3.1 Major Faults and Rupture in the Tangshan Region

The Tangshan earthquakes of 29 July 1976 ruptured a five-mile (8 km) section of a 25-mile strike-slip fault with a north-northeast orientation that passes through the city Tangshan (Fig. 4). The fault is part of an extensive strike-slip fault system, known as Tancheng-Ljiang, or Tan-Lu. This system extends in a north-northeast direction for more than 3,200 miles from the north bank of the Yangtze River in eastern China to the west across the Russian border.

Specifically, the 1976 earthquake occurred at the junction of the YanShan fold-fault zone and the Cangdong fault zone. The YanShan fold-fault zone runs in an east-west direction and lies north of the Tangshan region. To the south, there are several sub-parallel northeast-trending fault zones known as the Shanxi fault depression structural belt, the Taihang piedmont fault zone, the Cangdong fault zone, and the Tangcheng-Lijiang fault zone. According to the scientific literature, each of these zones has produced several earthquakes. Several episodes of uplift and other anomalous variations along different segments of the fault zones that comprise the Yan Shan Seismic Belt have been reported.

#### *3.1a The Yan Shan Seismic Zone*

The Tangshan earthquake occurred at the junction of the Tangshan fold-fault zone and the Cangdong fault zone. The YanShan fold-fault zone runs in an east-west direction and lies north of the Tangshan region. To the south, there are several sub-parallel northeast-trending fault zones known as the Shanxi fault depression structural belt, the Taihang piedmont fault zone, the Cangdong fault zone, and the Tangcheng-Lijiang fault zone. According to the scientific literature, each of these zones has produced several earthquakes. Several episodes of uplift and other anomalous variations along different segments of the fault zones that comprise the Yan Shan Seismic Belt have been reported. The significance of these anomalies remains to be further investigated as to the potential for future destructive earthquakes in the Beijing-Tianjin area, and for tsunami generation near the coasts in the Hebei Province and the Liaoning Province, north of Bohai Bay.

### 3.2 Ground Movements, Crustal Displacements and Fault Rupture of the Great 1976 Tangshan Earthquake

There were substantial ground movements along the segment of the fault that ruptured as a result of the Great Tangshan earthquake. Along the west side, the ground moved laterally for about 1,5 m in a north/northeast direction, sub-parallel to the major axis of the microseismic zone. However, in some areas, horizontal ground displacements of up to 7 meters were subsequently measured. On the eastern side of the rupture, the ground block tipped upward near the south end and downward at the northern end. As previously mentioned, the earthquake's intensities, the aftershock distribution, the crustal displacements, and the downward tilting at the southern end must have included a good portion of the Bohai Sea and the generation of a local tsunami.

The earthquake ruptured a five-mile (8 km) section of the 25-mile long fault that passes through the city Tangshan. The Tangshan Fault is a strike-slip fault with a north-northeast orientation. The fault is part of an extensive strike-slip fault system, known as Tancheng-Ljiang, or Tan-Lu. This system extends in a north-northeast direction for more than 3,200 miles from the north bank of the Yangtze River in eastern China to the west across the Russian border

## 4.0 HISTORIC EARTHQUAKES AND TSUNAMIS IN THE BOHAI BASIN REGION OF NORTH-EAST CHINA

The complex intra-plate earthquakes in Northern China have been extensively studied in the past by US institutions funded by the National Science Foundation's PIRE (Partnerships for International Research and Education) in close collaboration with numerous Chinese institutions. The studies included integration of seismic imaging of earth structure, geodetic measurement of crustal deformation, paleo-seismic reconstruction of earthquake histories, and geodynamic computer simulations. Such studies provided a better understanding as to the causes of large earthquakes in Northeast China, such as the destructive 1976 Tangshan event that leveled the city and caused the greatest death toll in recent history.

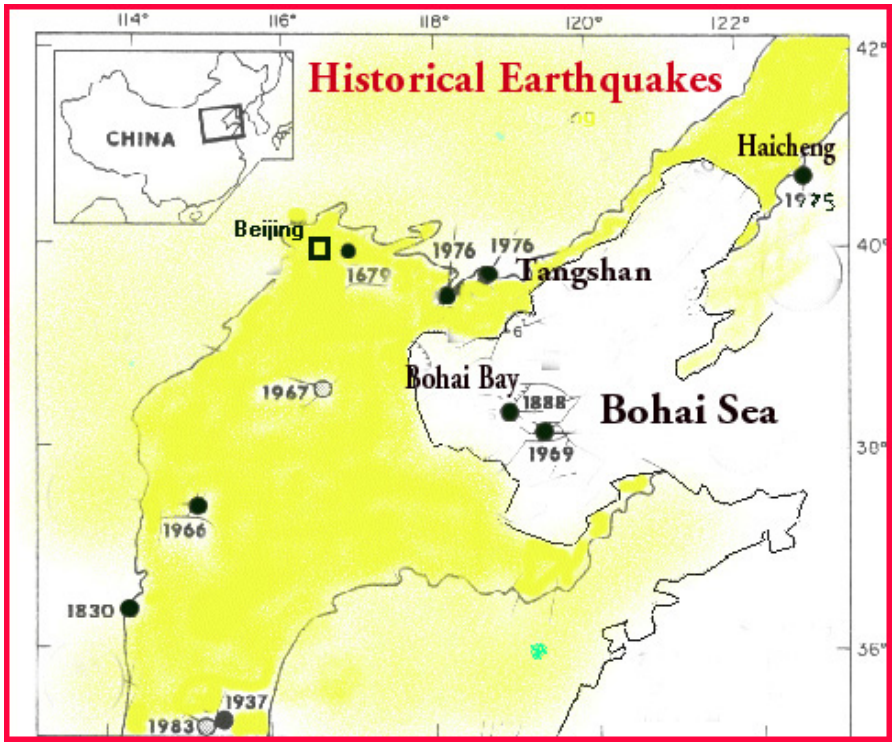


*Fig. 8. Historic earthquakes in the Bohai Sea in the Northeastern Margin of China.*

According to historical records, there have been six great earthquakes of Ms 8 magnitude and 16 major earthquakes of Ms 7 magnitude in the area of Northeast China, in the past 2000 years7 (Gu, 1983; Ma, 1988, Pararas-Carayannis. 2007). Earthquakes with Ms >7 have occurred in this region between 1966 and 1976 (see Fig. 8 above). Economic losses caused by these earthquakes were estimated to be about 10 billion yuan, but Tianjin city alone suffered about 7.5 billion Yen in direct and indirect damages, therefore even this figure is probably inaccurate. Historically, the Shaanxi Province massive earthquake of 23 January 1556 in northern China, with an estimated magnitude of M 8.0, is believed to be the deadliest ever recorded. It struck Shansi, China killing 830,000 people.

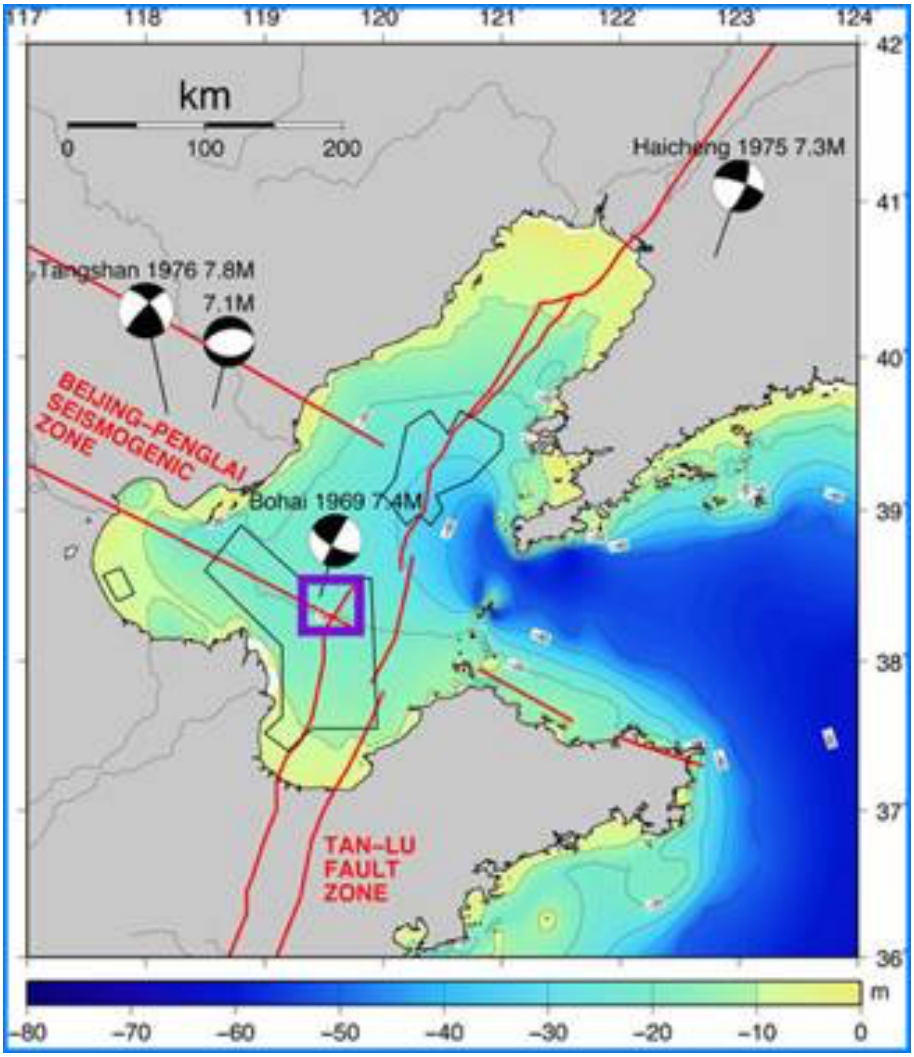


Fig. 9. *Major seismotectonic and seismogenic fault zones in the Bohai Basin and Sea. Earthquake epicenters and focal mechanisms of recent earthquakes. Bathymetry based on GEBCO digital data base* (after Pararas-Carayannis, 2009) (*modified graphic, after Yang & Xu, 2004 and Xu et al, 2004).*

The more recent earthquakes also resulted in hundreds of thousands of casualties and in significant economic damage. As mentioned, the worse of all recent events was the July 28, 1976, Tangshan earthquake. Generally, and as shown in Fig. 9, these large earthquakes have occurred along the major active faults that bound the Bohai Basin, but even within the Bohai Sea in 1888 and in 1969. Numerous strike-slip and normal faults on land in the Liaoning and Hebei Provinces are the predominant active structures where such very destructive earthquakes occur more frequently.

As previously indicated, the fault-plane solutions of historic earthquakes in the Bohai Basin area usually show right-lateral strike-slip with prominent NE orientation, although some had NW orientation with a normal dip-slip component. Recurrence frequencies in this region also have varied. Although earthquake recurrence intervals along any individual fault in the Bohai Basin are relatively long (usually in the range of several thousand years), the composite recurrence interval for the whole region is in the order of a few decades (Ma et al., 1989; Ma & Gao, 1996).

### 4.1 The 4 February 1975 Haicheng Earthquake and Tsunami

A previous major earthquake in the region occurred at 19:36 CST on 4 February 1975 South-Southeast of Haicheng, a town of approximately one million inhabitants in China's southern Liaoning Province (Fig. 9) The Haicheng earthquake and tsunami have been extensively studied (Chen, Y-T et al., 1976; Shou, 1999. Chen et al. 2007; Cipar 1979; Davis et al. 2001, Earthquake Administration of Liaoning 1975; Wang et al, 2006; Wang 2007; Pararas-Carayannis, 2008b). The quake had a shallow depth and $M_s$ magnitude of 7.5. In addition to damage in Liaoning Province and its surroundings, minor damage was also reported in Seoul, South Korea. The quak was felt in Primorsky Krai, Russia, and in Kyushu, Japan.

Although the quake caused total destruction of Haicheng's infrastructure and property, it did not result in many deaths because the earthquake had been successfully predicted and most inhabitants had evacuated the city earlier that day. The decision to evacuate was based on reports of continuing changes in groundwater and soil elevations over a long period, as well as widespread accounts of unusual animal behavior. The unusual animal behavior was observed earlier in December 1974. According to reports, rats and snakes appeared "frozen" on the roads. Also, starting in February 1975 reports of unusual animal behavior increased greatly. Cows and horses looked restless and agitated. Rats appeared "drunk", chickens refused to enter their coops and geese frequently took to flight . (Anonymous, 1977).

All these observations placed authorities on high alert, and earlier in the day on the 4th of February, ordered the evacuation of the city. Though this particular prediction of the earthquake was initially believed to be just the latest in a recent string of false alarms that had occurred in the preceding months, including one case of an earthquake swarm being caused by filling of a reservoir (Wang et al, 2006) the evacuation of Haicheng proceeded

anyway and eventually paid off. Local authorities ordered the evacuation of Haicheng early in the morning of 4 February. Nonetheless and in spite of the massive early evacuation that day, when the earthquake struck later at 7:36 p.m., 1,328 (some say 2,041) people died, over 27,000 were injured, as thousands of buildings collapsed. However, it was estimated that the death toll would have been at least 150,000 if there had been no evacuation at all.

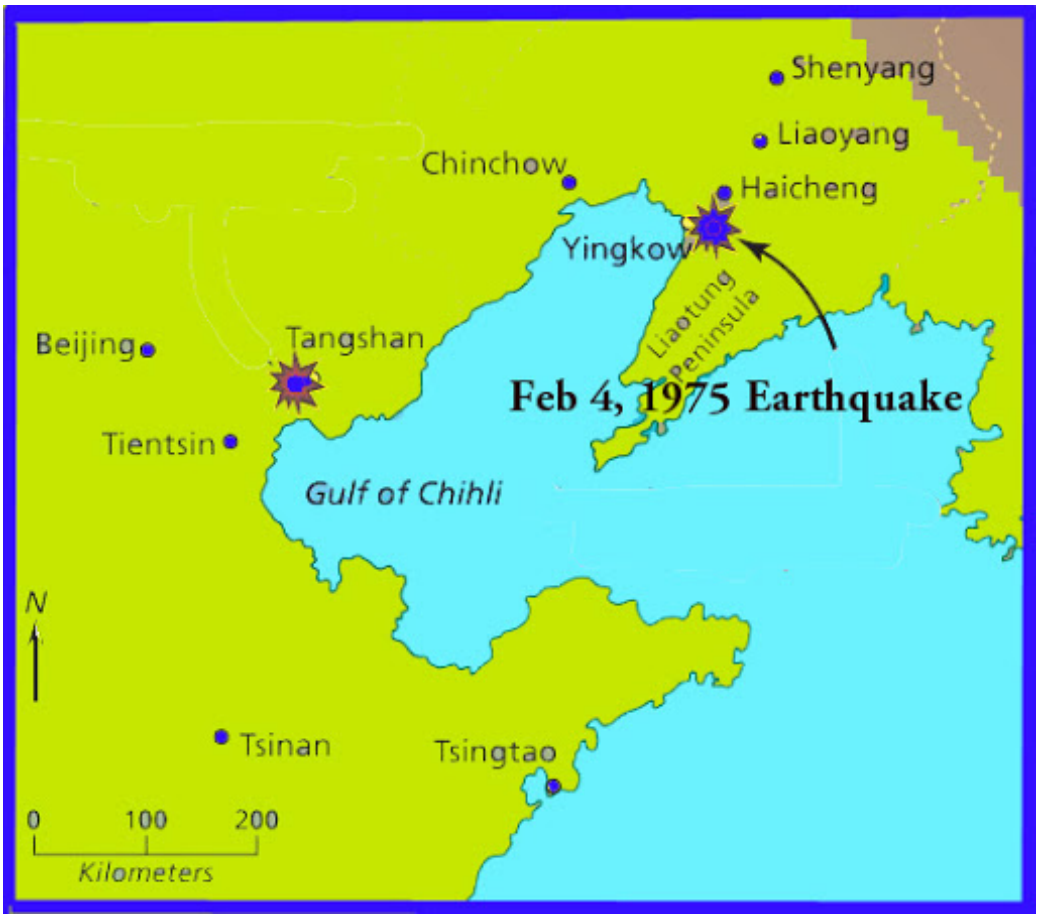


*Fig. 9. The 4 February 1975 Earthquake in Haicheng. Liaoning Province*

In recent years, the success of the earthquake's prediction has come under scrutiny (Ma, L. and Gao, X., 1996; Yin et al, 2000; Keilis-Borok & Soloviev, 2003). Seismologists have agreed that the Haicheng earthquake can't be looked to as any sort of "prototype" for predicting future earthquakes, as the foreshocks that played a huge role in leading to aprediction of this earthquake are not regular, reliable occurrences before all earthquakes. However, Qi-Fu Chen, a professor at Beijing's China Earthquake Administration, explained that this earthquake at least "showed the importance of public education," prompting a further discussion about the necessity of making the public aware of the dangers, of preparations, and of warning signs related to earthquakes (USGS, 2015 Historic Earthquakes)

## 5. TSUNAMI GENERATION IN THE BOHAI SEA FROM THE GREAT TANGSHAN EARTHQUAKE OF 28 JULY 1976

Infrequent earthquakes along active tectonic structures that crisscross the Bohai Basin near or within the Bohai Sea have generated local tsunamis in the past by a combination of direct and collateral mechanisms that involved not only strike-slip mechanisms but also tilting and upward or downward movements due to the folding of existing thick sedimentary layers, or the destabilization of gas hydrates deposits. Although most of the earthquakes in the Bohai Sea and the adjacent region, involve mainly lateral strike-slip components that do not contribute significantly to the generation of tsunamis, en-echelon structural failures and destabilization of existing gas hydrates deposits in the Bohai Sea have been postulated as being responsible for local tsunami generation (Pararas-Carayannis, 2008). Such mechanisms of the 28 July 1976 earthquake contributed to local tsunami generation as discussed in the following section.

### 5.1 Collateral En-Echelon Structural Failure Mechanisms of Tsunami Generation by the 28 July 1976 Earthquake - Partial Upward Block Displacement

As indicated by a previous study (Pararas-Carayannis, 2008), stress and tectonic displacements caused by an earthquake along a fault - whether strike-slip, normal, or inverse - in a multi-layered sedimentary environment such as that of the Bohai Sea - can cause structural failures that may be oblique to the overall fault orientation and thus result in collateral displacements, en-echelon structural failures, and bookshelf faulting of the seafloor, all of which could contribute to tsunami generation.

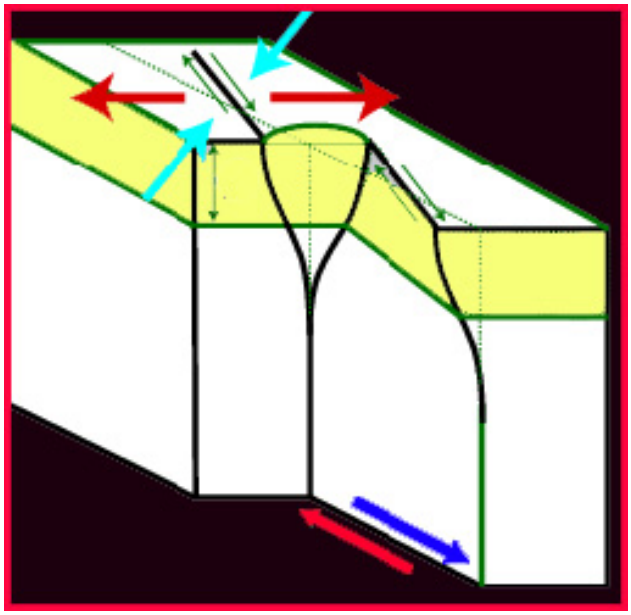

*Fig. 10. Stress concentration induced by strike-slip faulting across layer interfaces. (Modified Graphic http://hraun.vedur.is/ja/prenlab2final/img114.gif)*

The combination of high intensities of the 28 July 1976 earthquake, and of a localized upward block movement along the southern region of the affected source region, apparently contributed to folding of the thick sedimentary layers and to local tsunami generation in the Bohai Sea and adjacent region.

Fig. 10 above is an illustration of stress concentration which can be induced by strike-slip faulting across layer interphases of consolidated sedimentary layers. Shear cracks along a fault may be vertical and planar, but may also result in splits into two or more interacting sections at a stratigraphic interface with different density and stress drop - depending on rigidity contrasts between the adjoining media. Furthermore, the deeper sediments along faults in the Bohai Sea may be characterized by different elastic parameters, depending on the degree of hydration, particle size distribution, and compaction densities.

Also, a series of bookshelf type of structural failures may occur which will be oblique in orientations to the overall faulting trend. Oblique, en-echelon type of failures could result in multiple ruptures that could also affect the sediments of the upper layers - thus changing the spatial geometry and characteristics of the source area and the mechanism of tsunami generation. Slower rupture rates with different azimuthal orientation can be expected within these layers. Furthermore, net seafloor displacements can be expected to vary and the tsunami's directivity to be different from what may be inferred from fault orientation or focal plane solutions (Pararas-Carayannis, 2008).

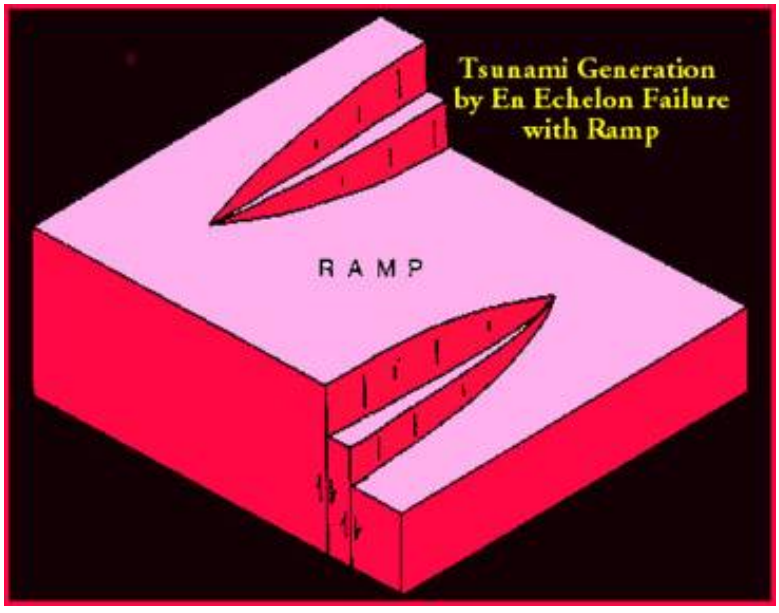


*Fig. 11. Tsunami Generation by En Echelon Step Fault Displacement and by Sea Floor Changes with Elevated and Depressed Ramp Structure (After Pararas-Carayannis, 2008).*

For example, the simplified mechanical/geometrical effects left by a model earthquake within a transform fault plane at the sedimentary discontinuity interphase have been extensively investigated by employing the "displacement discontinuity method" (Bonafede & Neri, 2000). Figure 11 illustrates a simple case of such stress-induced displacement discontinuity and the potential changes in the geometry and characteristics of the tsunami source. Additional investigations have dealt with the two-dimensional dynamics of yhe shallow reverse type of faulting upon discontinuity interphases (Madariaga, 2008).

However, in an actual multi-layered sedimentary environment such as that which exists in the Bohai Sea, the geometrical complexities and stress drop values can be expected to vary along planar strike-slip or reverse faults. Faulting in such an environment cannot remain planar. Strike-slip faulting at depth may be accompanied by en-echelon surface breaks in a shallow sedimentary layer - where the stress drop may be lower at the discontinuity interphase, while ductile deformation at depth may be accommodated by antithetic faulting in the upper brittle layer - enhanced with lower rigidity but higher stress - thus resulting in bookshelf faulting that can augment tsunami generation and alter tsunami directivity (Fig. 11), as indicated by earthquakes elsewhere. For example, bookshelf failure of sedimentary layers is believed to have resulted in the augmentation and apparent directivity from the north (rather than from the west) when the tsunami of December 26, 2004, struck Aceh, in Sumatra. It is believed that similar bookshelf and en-echelon failures within subducted sediments were also associated with the September 2, 1992 earthquake off the coast of Nicaragua and enhanced the tsunami run-up (Pararas-Carayannis, 1992). Indeed, studies of aftershock distribution of earthquakes around the world indicate an extensive concentration of their focal depths along sedimentary bedding planes - which would also support that such failure mechanisms contribute to tsunami enhancement and differences in azimuthal tsunami source parameters (Fig. 12).

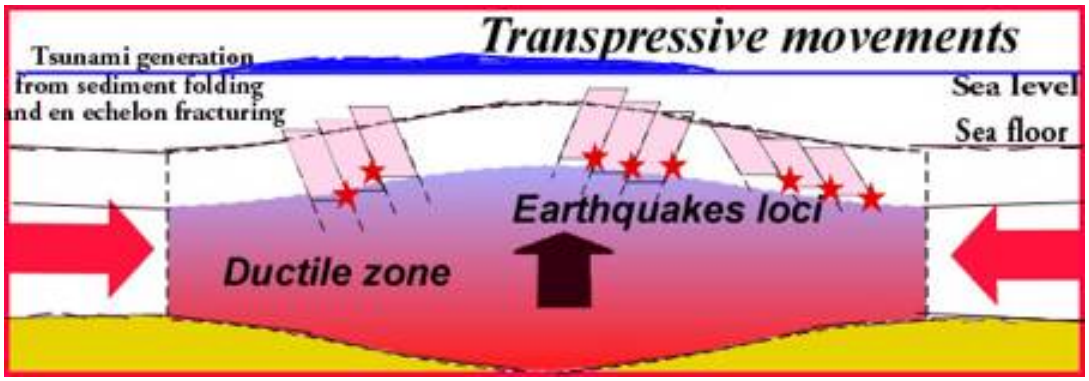


*Fig. 12.Transpressive Movements and Tsunami Generation from Sediment Folding and en-echelon fracturing.*

Therefore, we may conclude that such distribution of aftershocks of the 28 July 1976 earthquake - localized along with sedimentary discontinuity layers - not only indicates the asymmetric interactions between the original fault plane of the earthquake and the

shallower sedimentary layers, but also indicate that significant residual, compressive or tensile stresses remained over the shallower portion of the fault surface on the southern section, after the major shock and fault rupture. Thus, the strong aftershocks of the earthquake in the existing sedimentary environment of the Bohai Sea Basin contributed to local tsunami generation  In brief, tsunami generation in the Bohai Sea was exacerbated by the thick accumulation of sediments (in different states of consolidation) and the multi-layered stratigraphic distribution of such sediments, with different shear strengths, densities, and rigidities.  En-echelon, bookshelf type of failures with oblique directivity to the general strike orientation imparted greater tsunami energy and altered its directivity.

Finally, Tsunami Society International in 2002 held a Symposium in Honolulu, Hawaii where the existence of gas hydrates in submarine sedimentary formations was extensively reviewed. One of the papers, in particular that was presented pertained to the global distribution and significance in the petroleum industry of naturally occurring gas hydrates as well as of the associated risks (Milkov, 2002). The risks were also expanded in subsequent studies (Watson et al., 1987; Pararas-Carayannis, 2009).

As graphically illustrated by Fig. 13 below, there may have been some contribution to local tsunami generation from the dissociation of gas hydrate within the consolidated sedimentary zone which exists in the Bohai Bay area, where oil and gas extracting platforms did not exist in 1976. However, this is an area of great reserves of oil and gas in China.

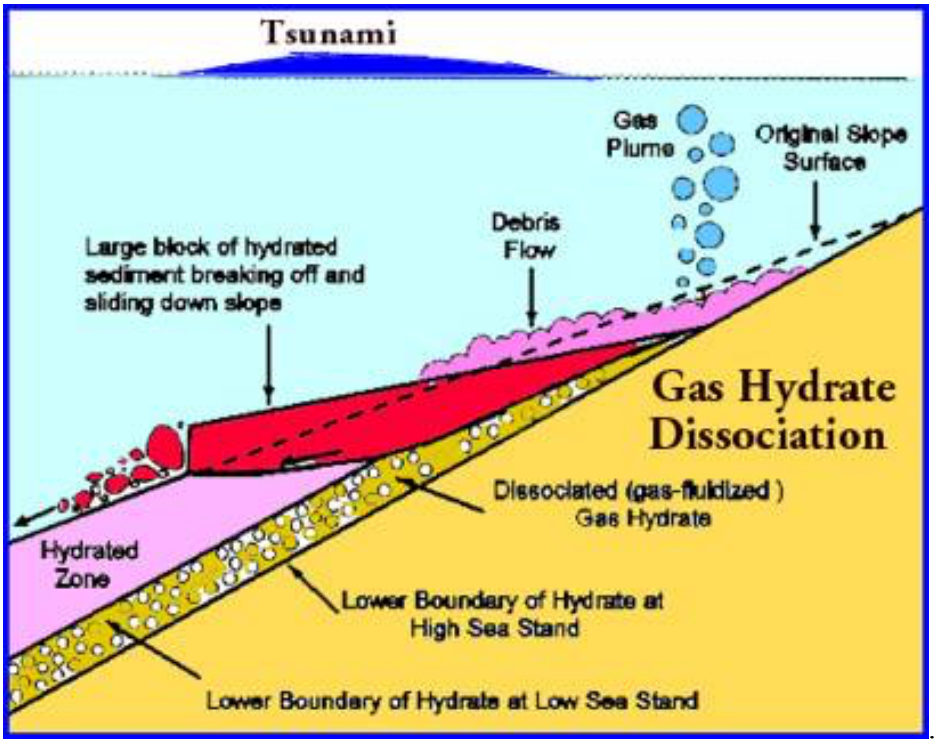


Fig. 13. Tsunami generation from Gas Hydrate dissociation within the sedimentary layers of a hydrated zone.

Presently there are several platforms operating at a water depth of about 90 feet (27.43 meters) in Bohai Bay, about 140 miles from the town of Tanggu and about 85 miles from the town of Dallan. However, and as pointed out, the Bohai Sea is shallow and the slope of its underwater bathymetry is rather gentle, so a massive landslide was unlikely to have occurred in 1976 when the Tangshan earthquake occurred, although future large earthquakes may contribute to tsunami generation and possible damage to such offshore platforms, particularly in winter months when there is an accumulation of ice on the surface of Bohai Bay (Zang et al, 2008) and a local tsunami could carry large pieces of broken ice that could strike and perhaps damage the supporting columns of the now existing oil and gas platforms or even break pipelines and ignite a fire similar to the "Deep Horizon" drilling rig explosion of 2010 in the Gulf of Texas

## CONCLUSIONS

The magnitude M7.8 earthquake of 28 July 1976 and its M7.1 major aftershock in the Hebei Province of Northern China were extremely catastrophic in the city of Tangshan and surrounding areas and resulted in more deaths than any other earthquake in recent times. Based on a review and analysis of the seismo-tectonics of the region, of earthquake intensities, of aftershock distribution, and of strike-slip ground motions of the major existing faults along the YanShan and the Cangdong fold-fault zones, the present study provides an explanation as to the extreme impact of this event. Although strike-slip earthquakes involve primarily lateral ground motions and do not generate tsunamis, this particular earthquake involved some downward tilting and crustal displacements of both consolidated and nonconsolidated sedimentary layers along the coasts of the Bohai Sea, which contributed to local tsunami generation within the Bohai Sea.

The Tangshan earthquake of 28 July 1976 involved mainly lateral strike-slip faulting ground motions which do not trigger tsunamis, but high-intensity ground motions associated with such strike-slip events near a coast can often trigger undersea landslides, which may result in significant tsunamis. The Bohai Sea is very shallow, so the 1976 earthquake-generated no significant landslides. However, the coastal geomorphology and the presence of consolidated sedimentary layers in the Bohai Basin region – some of the tilting - support local tsunami generation by the compression of such layers into bookshelf type of failure in a sequential manner by the lateral forces of the strike-slip earthquake. Such mechanism contributing to greater tsunamigenic efficiency was determined for the 2011 Japan earthquake and for the higher degree of that tsunami's destructiveness along Honshu Island's coastlines. The study of the 2011 event in Japan indicated that vertical crustal displacements of more than 10 m due to up-thrust faulting, were augmented by lateral compression and folding of sedimentary layers, thus contributing to additional uplift estimated at about 7 meters - mainly along the leading segment of the accretionary prism of the overriding tectonic plate, and thus contributing significantly to a tsunami of greater height (Pararas-Carayannis, 1983, 1993; 2011; 2013). Therefore, it is concluded that even

in the absence of major vertical displacements, the strike-slip motions of the 1976 Tangshan earthquake, the high up to XI intensities near and along the coasts of the Bohai Sea, and an upward crustal movement on the southern block of the area affected did contribute to tsunami generation, although difficult to determine quantitatively.

## REFERENCES


Bonafede, M.; Neri, A., 2000. Effects induced by an earthquake on its fault plane boundary element study. Geophysical Journal International, Volume 141, Issue 1, pp. 43-56, 2000.

Castellanos, H., and Mann, P., 2005. Pull-Apart vs. Subduction Rollback Mechanisms For The Cenozoic Formation Of Bohai Basin, Eastern China AGU Fall Meeting, San Francisco, CA. 2005.

Chen, Yun-Tai; Gu, Hao-Ding; Lu, Zao-Xun, 1976. "Variations of gravity before and after the Haicheng earthquake, 1975 and the Tangshan earthquake, 1976", Physics of the Earth and Planetary Interiors, Volume 18, Issue 4, p. 330-338.

Chen Guo-guang, Xu Jie, Ma Zong-jin1, Deng Qi-dong, Zhang Jin and Zhao Jun-meng, 2007. Recent tectonic stress field and major earthquakes of the Bohai sea basin, Acta Seismologica Sinica, Volume 17, Number 4 / July, 2004, pp.438-446, Published by Springer in Earth and Environmental Science, 2007.

Cipar J. 1979, "Source processes of the Haicheng, China earthquake from observations of P and S waves", Bulletin of the Seismological Society of America; December 1979; v. 69; no. 6; p. 1903-1916.

Davis, G. A., Zheng, Y., Wang, C., Darby, B. J., Zhang, C., and Gehrels, G., 2001, Mesozoic tectonic evolution of the Yanshan fold and thrust belt, with emphasis on Hebei and Lianoning provinces, northern China: Memoir - Geological Society of America, v. 194, p. 171-197.

Earthquake Administration of Liaoning Province, Quan Yingdao, "An Earthquake of MS7.3 in Haicheng, Liaoning Province on February 4, 1975", World Data Center for Seismology, Beijing.

Hellinger, S.J., Shedlock, K.M., Sclater, J.G. and H. Ye, 1985. The Cenozoic evolution of the north China basin, Tectonics 4 (1985) 343–358.

Hendrix, M.S., and Davis, G.A., 2001, Paleozoic and Mesozoic tectonic evolution of central Asia: from continental assembly to intracontinental deformation: Boulder, Colo., Geological Society of America, vi, 447 p.

Keilis-Borok, V. I. and Soloviev, A., (Edis.), 2003. Nonlinear Dynamics of the Lithosphere and Earthquake Prediction. Springer-Verlag, Berlin-Heidelberg.

Ma, L. and Gao, X., 1996. The state of intensive monitoring and prediction at the Metropolitan Area before Asian Game in 1990. He, Y. N. (Ed.), The Selected Papers of Earthquake Prediction in China, Dedicated to the 30 th International Geological Congress, Seismological Press, Beijing, 255-259.

Madariaga, Raul, 2008. Dynamics of shallow reverse faulting in 2D Max, Michael D. 2002, Mass Flow in Marine Sediment: Physical Causes and Possible Examples from the Geological Record, Tsunami Society Symposium, Honolulu, Hawaii 2002.

Mei, S. R. (Ed.), 1982. Tangshan Earthquake in 1976. Seismological Press, Beijing (in Chinese, reviewed abstract in English).

Milkov, Alexei V. 2002, Global Distribution and Significance of Natural Gas Hydrate. Tsunami Society Symposium, Honolulu, Hawaii 2002.

Pararas-Carayannis, G. (1983), *The Earthquake and Tsunami of 26 May 1983 in the Sea of Japan*. http://www.drgeorgepc.com/Tsunami1983Japan.html

Pararas-Carayannis, G. 1993. *The Earthquake and Tsunami of July 12, 1993 in the Sea of Japan/East Sea—The Hokkaido "Nansei-Oki" Earthquake and Tsunami*.http://www.drgeorgepc.com/Tsunami1993JAPANOkushiri.html

---

Pararas-Carayannis, G., 2007. Historical Earthquakes in China. Webpage Article: **http://www.drgeorgepc.com/EarthquakesChina.html**

Pararas-Carayannis, G. 2008.The_Great_Tohoku Oki Earthquake and Tsunami of 11 March 2011 in Japan – A Critical Review and_Evaluation of the Tsunami Source Mechanism. https://www.researchgate.net/publication/257317821

Pararas-Carayannis, G., 2008a, The Earthquake and Tsunami of July 18, 1969 in the Bohai Sea, China. Webpage Article: **http://drgeorgepc.com/Earthquake1969ChinaBohai.html**

Pararas-Carayannis, G., 2008b. The Earthquake of February 4, 1975 in Haicheng, China. Webpage Article:**http://drgeorgepc.com/Earthquake1975ChinaHaicheng.html**

Pararas-Carayannis, G., 2008c. The Tangshan Earthquake of July 28,1976 in China. Webpage Article: **http://drgeorgepc.com/Earthquake1976ChinaTangshan.html**

Pararas-Carayannis, G., 2009. Assessment of Potential Tsunami Generation in China's Bohai Sea from Direct Geotectonic and Collateral Source Mechanisms.Science of Tsunami Hazards. Vol. 18. N.1, 2009. http://tsunamisociety.org/281GPCC.pdf

Pararas-Carayannis, G. (2009), *Earthquake and Tsunami of 3 March 1933 in Sanriku, Japan.* http://drgeorgepc.com/Tsunami1933JapanSanriku.html .

Pararas-Carayannis, G. (2011), *The Great Tsunami of March 11, 2011 in Japan—Analysis of Source Mechanism and Tsunamigenic Efficiency*. OCEANS 11, MTS/IEEE Proceedings, 2011.

Pararas-Carayannis, G. (2013), The Great Tohoku-Oki Earthquake and Tsunami of March 11, 2011 in Japan: A Critical Review and Evaluation of the Tsunami Source Mechanism. Pure and Applied Geophysics, Volume 171, Issue 12, pp.3257, May 2013. DOI: 10.1007/s00024-013-0677-7

Pararas-Carayannis, G., 2007. Historical Earthquakes in China. Webpage Article: http://www.drgeorgepc.com/EarthquakesChina.html

Pararas-Carayannis, G., 2008a, The Earthquake and Tsunami of July 18, 1969 in the Bohai Sea, China. Webpage Article: http://drgeorgepc.com/Earthquake1969ChinaBohai.html

Pararas-Carayannis, G., 2008b. The Earthquake of February 4, 1975 in Haicheng, China. Webpage Article: http://drgeorgepc.com/Earthquake1975ChinaHaicheng.html

Pararas-Carayannis, G., 2008c. The Tangshan Earthquake of July 28,1976 in China. Webpage Article: http://drgeorgepc.com/Earthquake1976ChinaTangshan.html

Pararas-Carayannis, G. 2008d. The Earthquake of May 12, 2008 in the Sichuan Province of China. Website: http://www.drgeorgepc.com/Earthquake2008ChinaSichuan.html

Pararas Carayannis, G. 2009. ASSESSMENT OF POTENTIAL TSUNAMI GENERATION IN CHINA'S BOHAI SEA FROM DIRECT GEOTECTONIC AND COLLATERAL SOURCE MECHANISMS, Science of Tsunami Hazards, Vol.28 No 1. 2009. pp 35-66

Shou, Zhonghao 1999. "The Haicheng Earthquake and Its Prediction", Science and Utopya 65, page 34, November 1999" (in Turkish; Reviewed English abstract)
Science of Tsunami Hazards, Vol. 28, No. 1, page 64 (2009*)*

USGS.gov. 2015. "Historic Earthquakes". earthquake.usgs.gov. Retrieved 2015-11-

Ye, H., Shedlock, K.M., Hellinger, S.J. and J.G. Sclater, 1985. The north china basin: an example of a Cenozoic rifted intraplate basin, Tectonics 4 (1985) 153– 169.

Yin, X. C., Wang, Y. C., Peng, K. Y. and Bai, Y. L., 2000. Development of a new approach to earthquake prediction: Load/Unload Response Ratio (LURR) theory. Pure Appl. Geophys. 157, 2365-2383.

Yin, A., and Nie, S., 1996, A Phanerozoic palinspastic reconstruction of China and its neighboring regions, in Yin, A., and Harrison, T. M., eds., The Tectonic evolution of Asia: Cambridge [England] ; New York, Cambridge University Press, p. 442-485.

Yong, Chen, et al.,1988. The Great Tangshan Earthquake of 1976: An Anatomy of Disaster. New York: Pergamon Press, 1988**.**

Yu Jianguo, Li Sanzhong, Wang Jinduo, Timothy M. Kusky ; Wang Xinhong ; Lu Shengqiang, 1995. Relationship between salt diapirism and faulting in the central structural belt of the Dongying sag, Bohai Gulf basin, ChinaQuaternary International Volume 25, 1995, Pages 13- 17.

Wang Fang, 1976. The 1976 Tangshan Earthquake. State Seismological Bureau of China Beijing, People's Republic of China.

Wang, Kelin; Chen, Qi-Fu; Sun, Shihong; Wang, Andong (2006). "Predicting the 1975 Haicheng Earthquake". Bulletin of the Seismological Society of America. **96**(3): 757–795. *doi*:*10.1785/0120050191*.

Zhang, Z.M., Liou, J.G., and Coleman, R.G., 1984, An outline of the plate tectonics of China: Geological Society of America Bulletin, v. 95, p. 295-312.
Wang, K., Chen,Q.-F., Sun, S. and A. Wang, 2006, Predicting the 1975 Haicheng Earthquake, Bulletin of the Seismological Society of America, June 1, 2006; 96(3): 757 - 795.

Wang Jian, 2007. Historical earthquakes and a tsunami in Bohai Sea. Journal Acta Seismologica Sinica. Publisher Seismological Society of China ISSN 1000-9116 (Print) 1993-1344 (Online), Volume 20, Number 5 / September, 2007.

Wang, T.H., 1988. Genetic types of thrust faults in Eastern China petroliferous regions, Earth Sci. 13 (1988) 627– 634.

Wang Fang, 1976. The 1976 Tangshan Earthquake. State Seismological Bureau of China Beijing, People's Republic of China.

Watson, M.P., Hayward, A.B., Parkinson, D.N. and Z. Zhang, 1987. Plate tectonic evolution, basin development and petroleum source rock deposition onshore China, Mar. Pet. Geol. 4 (1987) 205– 225.

Xu Qinghai, Wu Chen, Yang Xiaolan and Zhang Ningjia, 1996. Palaeochannels on the North China Plain: relationships between their development and tectonics. Studies of the Palaeochannels on the North China Plain, Geomorphology, Volume 18, Issue 1, December 1996, Pages 27-35.

Zhang D., and S. Wang, 2008, Failure modes analyses of ice-resist jacket platforms in Bohai Sea. Dalian University of Technology, Dalian 116024, China ( Abstract seen)

Zhao Liang and Tianyu Zheng, 2005, Seismic structure of the Bohai Bay Basin, northern China: Implications for basin evolution. Earth and Planetary Science Letters 231, Issues 1-2 (Feb. 2005) Pages 9– 22.

ISSN 8755-6839

# SCIENCE OF **TSUNAMI HAZARD**

Journal of Tsunami Society International

**Volume 40** **Number 2** **2021**



WWW.TSUNAMISOCIETY.ORG

*TSUNAMI SOCIETY INTERNATIONAL, 1741 Ala Moana Blvd. #70, Honolulu, HI 96815, USA*.

WWW.TSUNAMISOCIETY.ORG